



## 1 **Impact of a moderate volcanic eruption on chemistry in the lower** 2 **stratosphere: balloon-borne observations and model calculations**

3 Gwenaél Berthet<sup>1</sup>, Fabrice Jégou<sup>1</sup>, Valéry Catoire<sup>1</sup>, Gisèle Krysztofiak<sup>1</sup>, Jean-Baptiste Renard<sup>1</sup>, Adam  
4 E. Bourassa<sup>2</sup>, Doug A. Degenstein<sup>2</sup>, Colette Brogniez<sup>3</sup>, Marcel Dorf<sup>4</sup>, Sebastian Kreycky<sup>4</sup>, Klaus  
5 Pfeilsticker<sup>4</sup>, Bodo Werner<sup>4</sup>, Franck Lefèvre<sup>5</sup>, Tjarda J. Roberts<sup>1</sup>, Thibaut Lurton<sup>1</sup>, Damien Vignelles<sup>1</sup>,  
6 Nelson Bègue<sup>6</sup>, Quentin Bourgeois<sup>7</sup>, Daniel Daugeron<sup>1</sup>, Michel Chartier<sup>1</sup>, Claude Robert<sup>1</sup>, Bertrand  
7 Gaubicher<sup>1</sup>, and Christophe Guimbaud<sup>1</sup>

8 <sup>1</sup>Laboratoire de Physique et Chimie de l'Environnement et de l'Espace (LPC2E), Université d'Orléans, CNRS  
9 UMR7328, Orléans, France

10 <sup>2</sup>Institute of Space and Atmospheric Studies, University of Saskatchewan, Saskatoon, Canada

11 <sup>3</sup>Laboratoire d'Optique Atmosphérique, Université Lille 1 Sciences et Technologies, CNRS UMR8518,  
12 Villeneuve d'Ascq, France

13 <sup>4</sup>Institute of Environmental Physics, University of Heidelberg, Heidelberg, Germany

14 <sup>5</sup>Laboratoire Atmosphères Milieux Observations Spatiales, UPMC, Université Paris 06, Université Versailles  
15 Saint Quentin, CNRS UMR8190, LATMOS-IPSL, Paris, France

16 <sup>6</sup>Laboratoire de l'Atmosphère et des Cyclones, UMR8105 CNRS, Université de la Réunion, France

17 <sup>7</sup>Department of Meteorology and Bolin Centre for Climate Research, Stockholm University, Stockholm, Sweden

18

19

20

### 21 **Abstract.**

22 The major volcanic eruption of Mount Pinatubo in 1991 has been shown to have significant effects  
23 on stratospheric chemistry and ozone depletion even at mid-latitudes. Since then, only “moderate” but  
24 recurrent volcanic eruptions have modulated the stratospheric aerosol loading such as the eruption of  
25 the mid-latitude Sarychev volcano which injected 0.9 Tg of sulfur dioxide (about 20 times less than  
26 Pinatubo) in June 2009. In this study, we investigate the chemical impacts of the enhanced liquid  
27 sulfate aerosol loading resulting from this moderate eruption using data from a balloon campaign  
28 conducted in northern Sweden (Kiruna-Esrange, 67.5°N, 21.0°E) in August-September 2009. Balloon-  
29 borne observations of NO<sub>2</sub>, HNO<sub>3</sub> and BrO from infrared and UV-visible spectrometers are compared  
30 with the outputs of a three-dimensional (3D) Chemistry-Transport Model (CTM). It is shown that  
31 differences between observations and model outputs are not due to transport calculation issues but  
32 rather reflect the chemical impact of the volcanic plume below 19 km in altitude. Good measurement-  
33 model agreement is obtained when the CTM is driven by volcanic aerosol loadings derived from in  
34 situ or space-borne data. As a result of enhanced N<sub>2</sub>O<sub>5</sub> hydrolysis in the Sarychev volcanic aerosol  
35 conditions, the model calculates reductions of ~45% and increases of ~11% in NO<sub>2</sub> and HNO<sub>3</sub>  
36 amounts respectively over the summer 2009 period. The decrease in NO<sub>x</sub> abundances is limited due to  
37 the expected saturation effect for high aerosol loadings. The links between the various chemical  
38 catalytic cycles involving chlorine, bromine, nitrogen and HO<sub>x</sub> compounds in the lower stratosphere  
39 are discussed. The increased BrO amounts (~22%) compare rather well with the balloon-borne  
40 observations when volcanic aerosol levels are accounted for in the CTM and appear to be mainly  
41 controlled by the coupling with nitrogen chemistry rather than by enhanced BrONO<sub>2</sub> hydrolysis.  
42 Simulated effects of the Sarychev eruption on chlorine activation and partitioning are very limited in  
43 the high temperature conditions in the stratosphere at the period considered, inhibiting the effect of  
44 ClONO<sub>2</sub> hydrolysis. As a consequence, the simulated ozone loss due to the Sarychev aerosols is low  
45 with a reduction of 1.1% of the ozone budget at 16.5 km. Some comparisons with the reported  
46 Pinatubo chemical impacts are also provided and overall the Sarychev aerosols have led to less  
47 chemical effects than the Pinatubo event.



## 1 1. Introduction

2

3 In the stratosphere, the photo-oxidation of N<sub>2</sub>O is the main source of the total nitrogen species (NO<sub>y</sub>).  
4 About 97% of the stratospheric NO<sub>y</sub> budget can be explained by the NO, NO<sub>2</sub>, HNO<sub>3</sub>, ClONO<sub>2</sub>, and  
5 N<sub>2</sub>O<sub>5</sub> compounds and the partitioning between reactive and reservoir nitrogen species is an important  
6 issue in stratospheric ozone chemistry (e.g. Wetzel et al., 2002; Brohede et al., 2008). Nitrogen oxides  
7 (NO<sub>x</sub> = NO + NO<sub>2</sub>) are major catalysts responsible for significant ozone destruction in the middle  
8 stratosphere. In the gas phase, NO<sub>x</sub> interacts with the hydrogen and halogen species in catalytic cycles  
9 affecting ozone loss rates in the lower stratosphere (e.g. Portmann et al., 1999; Salawitch et al., 2005).  
10 Therefore NO<sub>x</sub> can also buffer the ozone destruction by halogenated compounds through the formation  
11 reaction of ClONO<sub>2</sub> and BrONO<sub>2</sub> (e.g. Rivière et al., 2004). The HNO<sub>3</sub> reservoir is formed from NO<sub>x</sub>  
12 indirectly via the hydrolysis of N<sub>2</sub>O<sub>5</sub> on liquid sulfate aerosols:

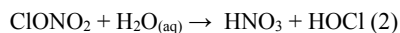
13



15 It has been shown that models need to include reaction (1) to better reproduce observations of NO<sub>y</sub>  
16 partitioning at mid-latitude for background aerosol conditions (i.e. in volcanically quiescent periods) in  
17 the lower stratosphere (Rodriguez et al., 1991; Granier and Brasseur, 1992; Fahey et al., 1993; Webster  
18 et al., 1994; Salawitch et al., 1994b; Sen et al., 1998). This reaction tends to decrease NO<sub>x</sub> amounts and  
19 reduces the ozone loss efficiency associated with the NO<sub>x</sub> catalytic cycle as the less reactive nitrogen  
20 reservoir HNO<sub>3</sub> is formed (e.g. Rodriguez et al., 1991; Weisenstein, 1991; McElroy et al., 1992).  
21 Reaction (1) is fairly insensitive to temperature and has the potential to greatly reduce reactive nitrogen  
22 globally, even under background aerosol conditions.

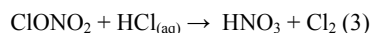
23 The hydrolysis of ClONO<sub>2</sub> can be expressed by:

24



25 It results in additional formation of HNO<sub>3</sub> on sulfate aerosols and to the formation of reactive chlorine  
26 in the sunlight where HOCl is rapidly photolyzed releasing Cl radicals (e.g. Hofmann and Solomon,  
27 1989; Prather, 1992; McElroy et al., 1992). This heterogeneous reaction is highly dependent on the water  
28 content in the aerosols and has been shown to be of considerable importance in determining the  
29 abundance of active chlorine available to destroy ozone under some conditions, i.e. for temperatures  
30 typically below 210-215 K and where HNO<sub>3</sub> photolysis rates are slow (typically in winter at high  
31 latitudes), (e.g. Hanson et al., 1994; Tie et al., 1994; Borrmann et al., 1997). However, for higher  
32 temperatures the ClONO<sub>2</sub> hydrolysis is not expected to be significant enough to compete with reaction  
33 (1) on the NO<sub>y</sub> partitioning under these conditions (Fahey et al., 1993; Cox et al., 1994; Sen et al., 1998).  
34 Also, the reaction,

35

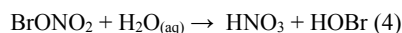


36

37 of ClONO<sub>2</sub> with dissolved HCl in sulfuric acid droplets have negligible effects on chlorine activation at  
38 such temperatures (Hanson et al., 1994; Borrmann et al., 1997).

39 Some works also suggest that the hydrolysis of BrONO<sub>2</sub>,

40



41

42

43 on background sulfate aerosols also plays a significant role in ozone depletion in the lower stratosphere  
44 with rates almost independent of temperature making this reaction efficient at all latitudes and for all  
45 seasons (Hanson and Ravishankara, 1995; Hanson et al., 1996; Lary et al., 1996; Randeniya et al., 1997;  
46 Erle et al., 1998).

47 After large volcanic eruptions, the aerosol loading in the stratosphere and the surface area densities  
48 (hereafter SAD) available for reaction (1) to occur are dramatically enhanced (e.g. Deshler et al., 2003).  
49 As a result, the amount of ozone-depleting NO<sub>x</sub> is strongly reduced (e.g. Prather, 1992; Johnston et al.,  
50 1992; Fahey, 1993; Mills et al., 1993; Solomon et al., 1994; Kondo et al., 1997; Sen et al., 1998) whereas  
51 HNO<sub>3</sub> amounts increase (Koike et al., 1993; Webster et al., 1994; Koike et al., 1994; Rinsland et al.,



1 2003) as shown for the Pinatubo aerosols. Different impacts on stratospheric ozone are expected  
2 depending on the altitude. In the middle stratosphere (above ~30 hPa) where ozone loss is dominated by  
3  $\text{NO}_x$ , the presence of volcanic aerosols can result in layers of increased net production of ozone due to  
4 the suppression of the  $\text{NO}_x$  cycle by the  $\text{N}_2\text{O}_5$  hydrolysis (Hofmann et al., 1994; Bekki and Pyle, 1994;  
5 Tie and Brasseur, 1995). In the lower stratosphere, halogen ( $\text{ClO}_x$  and  $\text{BrO}_x$ ) and hydrogen ( $\text{HO}_x$ )  
6 radicals play a dominant role in ozone depletion and their abundances, which depend on  $\text{NO}_x$  levels, are  
7 increased (in particular for halogen species, as the rate of gas-phase conversion of  $\text{ClO}$  into the  $\text{ClONO}_2$   
8 reservoir is reduced), resulting in an enhanced catalyzed ozone loss (McElroy et al., 1992; Granier and  
9 Brasseur, 1992; Brasseur and Granier, 1992; Hofmann et al., 1994; McGee et al., 1994; Bekki and Pyle,  
10 1994; Salawitch et al., 1994a; 2005; Tie et al., 1994; Solomon et al., 1996; Solomon, 1999).

11 However, the  $\text{NO}_x$ -to- $\text{HNO}_3$  conversion by reaction (1) shows saturation as the aerosol SAD  
12 increases because the amount of  $\text{N}_2\text{O}_5$  present in the stratosphere is limited by its production rate by the  
13 gaseous reaction  $\text{NO}_2 + \text{NO}_3$  (Fahey, 1993; Prather, 1992; Mills et al., 1993; Tie et al., 1994; Solomon  
14 et al., 1996; Kondo et al., 1997; Sen et al., 1998). Consequently, ozone loss rates are expected to be  
15 limited because the saturation of the  $\text{NO}_x/\text{NO}_y$  response to the aerosol increase dampens the increase in  
16  $\text{ClO}/\text{Cl}_y$  (Fahey et al., 1993; Tie et al., 1994). Reaction (2) does not show such a rapid saturation resulting  
17 in enhanced ozone depletion by chlorine catalytic cycles in cold air masses as the aerosol loading  
18 increases (Fahey et al., 1993). The  $\text{BrONO}_2$  hydrolysis through reaction (3) is primarily dependent on  
19 the aerosol loading and is enhanced in periods of high volcanic aerosol loading. The resulting increase  
20 of  $\text{BrO}_x$  and  $\text{HO}_x$  radical concentrations and decrease in  $\text{HCl}$  (due to enhanced  $\text{OH}$ ) accompanied by an  
21 increase in  $\text{ClO}_x$  radicals is expected to give further ozone loss in the lower stratosphere at all latitudes  
22 and seasons (Lary et al., 1996).

23 The year-to-year variability of ozone at northern mid-latitudes appears closely linked to changes in  
24 chlorine partitioning driven by volcanic aerosols from major eruptions, with stronger effects than solar  
25 cycle contributions on the mid-latitude ozone depletion (Solomon et al., 1999 and references therein).  
26 This is expected in periods with a stratosphere perturbed by elevated chlorine levels from anthropogenic  
27 activities (Tie and Brasseur, 1995; Solomon et al., 1996). In the past decade no event comparable to the  
28 Pinatubo or El Chichon eruptions was observed. However, several volcanic eruptions, though of much  
29 lesser amplitude, impacted the aerosol burden in the lower stratosphere over periods of months (Vernier  
30 et al., 2011). These "moderate" eruptions have occurred in a period of still high chlorine loading with  
31 potential impact on stratospheric ozone chemistry.

32 In this paper, we study the chemical impact of a short-term change in the amount of stratospheric  
33 sulfate aerosols resulting from one of these "moderate" volcanic eruptions on some key aspects of  
34 stratospheric chemistry and on ozone loss. The eruption of the Sarychev volcano on 15 and 16 June  
35 2009 provides a very good opportunity to conduct such an investigation because 0.9 Tg of sulfur dioxide  
36 were injected in the lower stratosphere (Clarisse et al., 2012) resulting in enhanced sulfate aerosol  
37 loading and surface area densities up to 19 km for a period of about 8 months (Jégou et al., 2013). The  
38 approach consists in analyzing the effect of the heterogeneous chemical reactions associated with  
39 enhanced sulfate aerosol amounts on the lower stratospheric composition from balloon-borne  
40 observations conducted in August-September 2009 from Kiruna in Northern Sweden (67.5°N, 21.0°E)  
41 and aerosol-constrained simulations using a 3D Chemistry Transport Model (CTM). We show that at  
42 the period of the measurements  $\text{N}_2\text{O}_5$  has reformed and the role of its hydrolysis becomes important  
43 again after the sunlit summer period. Here we estimate the ozone loss and discuss its amplitude in  
44 comparison with the effect of the Pinatubo eruption.

45

46

47

48

49

50



## 1 **2. Methodology**

2

### 3 **2.1 Balloon-borne observations**

4 Our study is based on in situ and remote-sensing balloon-borne observations obtained during summer  
5 2009 in Northern Sweden. More details about the instrument descriptions and retrieval techniques are  
6 given in the Appendix and in the references.

#### 7 **2.1.1 In situ observations**

8

9  
10 Aerosol in situ measurements have been performed by the STAC (Stratospheric and Tropospheric  
11 Aerosol Counter) instrument which is an optical particle counter providing aerosol size distributions  
12 (Ovarlez and Ovarlez, 1995; Renard et al., 2008). This instrument has been used in a number of studies  
13 dedicated to the quantification of the aerosol content in the stratosphere at various locations and seasons  
14 (e.g. Renard et al., 2002; Renard et al., 2010). Eight vertical aerosol concentration profiles have been  
15 observed between August and September 2009 as reported by Jégou et al. (2013).

16 We focus here on the in situ vertical profiles of  $\text{N}_2\text{O}$ ,  $\text{NO}_2$  and  $\text{HNO}_3$  provided by the SPIRALE  
17 (French acronym for SPectroscopie InfraRouge d'Absorption par Lasers Embarqués) infrared  
18 absorption spectrometer (Moreau et al., 2005) from two balloon flights. Firstly, the measurements during  
19 the 7 August 2009 flight (further on called SPIRALE-07082009) were conducted between 02:00 UT  
20 (04:00 local time) and 03:20 UT (05:20 local time) corresponding to altitudes of 14 km and 34 km  
21 respectively. The position of the balloon varied from  $67.72^\circ\text{N}$ - $21.40^\circ\text{E}$  to  $67.63^\circ\text{N}$ - $20.92^\circ\text{E}$  during the  
22 ascent. Secondly, the SPIRALE balloon flight on 24 August 2009 (further on SPIRALE-24082009, the  
23 measurements started at 21:00 UT (23:00 local time) at an altitude of 14 km and the maximum altitude  
24 of 34 km was reached at 22:30 UT (00:30 local time). The measurement position remained rather  
25 constant during the ascent with a displacement of the balloon from  $67.91^\circ\text{N}$ - $21.09^\circ\text{E}$  to  $67.86^\circ\text{N}$ -  
26  $20.94^\circ\text{E}$ . The data used in this study are averaged over a vertical range of 250 m (corresponding to ~1  
27 minute of measurements).

28

#### 29 **2.1.2 Remote-sensing observations**

30

31 Since 1996 stratospheric  $\text{NO}_2$  and BrO have been measured by solar occultation by the DOAS  
32 balloon-borne instrument using the so-called Differential Optical Absorption Spectroscopy (DOAS)  
33 technique (e.g. Platt, 1994; Stutz and Platt, 1996; Ferlemann et al., 2000). The details of the vertical  
34 profile retrieval can be found in Butz et al. (2006) for  $\text{NO}_2$  and in Harder et al. (1998), Aliwell et al.  
35 (2002), Dorf et al. (2006b) and Kreyey et al. (2013) for BrO. In our study we use the DOAS profile  
36 recorded in the stratosphere during the balloon ascent on 7 September 2009 between 15:15 UT (17:15  
37 local time) and 16:35 UT (18:35 local time), corresponding to altitudes of 10 km and 30 km respectively.

38 The SALOMON (French acronym for "Spectroscopie d'Absorption Lunaire pour l'Observation des  
39 Minoritaires Ozone et  $\text{NO}_x$ ") balloon-borne UV-visible spectrometer also uses the DOAS method to  
40 derive the mixing ratio profile of  $\text{NO}_2$  (Renard et al., 2000; Berthet et al., 2002). SALOMON was  
41 initially based on the lunar occultation technique but on 25 August 2009, we flew a new version also  
42 able to use the Sun as direct light source to derive BrO amounts. The profiles used in this study have  
43 been obtained on 25 August 2009 during solar occultation between 18:50 UT (20:50 local time) and  
44 19:30 UT (21:30 local time). The float altitude was of 33 km and the position of the tangent point varied  
45 from  $71.0^\circ\text{N}$ - $13.3^\circ\text{E}$  to  $71.4^\circ\text{N}$ - $12.6^\circ\text{E}$  for altitudes below 19 km which are the main focus of our study  
46 as a result of the presence of the volcanic aerosols.

47 Variations of solar zenith angle (SZA) along solar occultation lines of sight and associated  
48 concentration variations are likely to impact the retrieved vertical profiles near sunrise and sunset  
49 especially below 20 km (Newchurch et al., 1996; Ferlemann et al., 1998). This effect can be corrected  
50 using a photochemical model (e.g. Payan et al., 1999; Harder et al., 2000; Butz et al., 2006). However,  
51 some retrievals from occultation measurements do not include corrections for diurnal variations in



1 concentrations because such corrections are strongly dependent on the photochemical model used in the  
2 retrieval algorithm and are likely to result in additional errors (Randall et al., 2002).

3 In our study, the NO<sub>2</sub> profile from SALOMON instrument was recorded on 25 August 2009 from a  
4 typical solar occultation at constant float altitude. Applying a photochemical correction to convert the  
5 NO<sub>2</sub> concentrations to values expected at 90° SZA results in differences of only 3%. This calculation is  
6 in agreement with the work of Payan et al. (1999) who have reported differences of less than 6% between  
7 photo-chemically corrected and non-corrected profiles of NO<sub>2</sub>. We note that Bracher et al. (2005) have  
8 estimated larger diurnal variation effects, i.e. of about 10%. In the following the SALOMON  
9 uncorrected profile is used for comparisons with model outputs. The vertical profile observed by the  
10 DOAS instrument was recorded on 7 September 2009 with a different observation geometry, i.e. during  
11 the balloon ascent. In this case applying a photochemical correction gives differences of 24% and the  
12 model-measurement comparison must be done for an SZA = 90°. Photochemical effects on the BrO  
13 profile obtained by the SALOMON instrument from solar occultation measurements are estimated to be  
14 of 10% and are taken into account in the error estimation in accordance with the study of Ferlemann et  
15 al. (1998). Photochemical changes in the BrO SCDs recorded during balloon ascent are small and the  
16 DOAS BrO profile has not been corrected to 90°SZA (Ferlemann et al., 1998; Harder et al., 2000; Dorf  
17 et al., 2006b).

18  
19

## 20 2.2 Model calculations

21 The REPROBUS 3D CTM has been used in a number of studies of stratospheric chemistry involving  
22 nitrogen and halogen compounds in particular through comparisons with space-borne and balloon-borne  
23 observations (e.g. Krecl et al., 2006; Berthet et al., 2005; Brohede et al., 2007). It is designed to perform  
24 annual simulations as well as detailed process studies. A description of the model is given in Lefèvre et  
25 al. (1994) and Lefèvre et al. (1998), as well as in the Appendix.

26 In this study, REPROBUS was integrated from 1 October 2008 to 1 October 2009 with a horizontal  
27 resolution of 2° latitude by 2° longitude. The ozone field was initialized on 1 April 2009 from the  
28 ECMWF ozone analysis. We have conducted a REPROBUS simulation (hereafter called Ref-sim)  
29 constrained with typical background aerosol levels inferred from the 2D model and used as reference,  
30 namely without presence of volcanic aerosols. A simulation (hereafter called Sat-sim) has been set up  
31 by prescribing time-dependent variations of the stratospheric sulfate aerosol content from 1-km vertical  
32 resolution extinction measurements by the Optical Spectrograph and Infrared Imaging System (OSIRIS)  
33 instrument onboard the Odin satellite. OSIRIS aerosol extinction data used in this study are the validated  
34 version 5 retrieved at 750 nm (Bourassa et al., 2012). They compare well with the profiles inferred from  
35 the STAC balloon-borne aerosol counter (Jégou et al., 2013) thus providing confidence in the use of the  
36 data as a basis for consideration of time dependent changes of aerosol content. OSIRIS data have been  
37 averaged daily and zonally over 10° latitude bins. A standard Mie scattering model (Van de Hulst, 1957;  
38 Wiscombe, 1980; Steele and Turco, 1997) has been run to convert extinction values to H<sub>2</sub>SO<sub>4</sub> mixing  
39 ratios from parameters of log-normal unimodal size distributions provided by the STAC instrument and  
40 used in the work of Jégou et al. (2013) in the Sarychev aerosol conditions. The derived 3D H<sub>2</sub>SO<sub>4</sub> mixing  
41 ratios have been then incorporated into the model over the period of presence of the Sarychev aerosols  
42 in the northern hemisphere lower stratosphere, i.e. from the beginning of July 2009 onwards. The  
43 simulation has been conducted until October 2009 because OSIRIS data at high latitudes are lacking  
44 beyond this period due to decreasing solar illumination.

45 We have conducted another simulation (hereafter called Bal-sim) driven by aerosol observations with  
46 a slightly different approach. The method here consists in adjusting the H<sub>2</sub>SO<sub>4</sub> mixing ratios in the model  
47 to reproduce the range of SADs observed by the STAC aerosol counter in summer (Jégou et al., 2013).  
48 These observed SAD values are used as reference from the beginning of August until the end of the  
49 model run and are homogeneously distributed for latitudes above 40°N. This simplification is supported  
50 by the similar aerosol SAD values observed by Kravitz et al. (2011) at a different mid-latitude location  
51 in November 2009, i.e. ~2 months after the STAC measurements as mentioned by Jégou et al. (2013).  
52 Also, the SO<sub>2</sub> plume rapidly converts into aerosol sulfate, spreads out over the hemisphere and appears  
53 rather uniformly distributed from about the end of July (Haywood et al., 2010). Our computed  
54 uniformity of enhanced levels of SAD from August to September 2009 is representative, at least to some



1 extent, of the geographical distribution of the optical depth signal observed by the CALIOP/CALIPSO  
2 space-borne lidar over the northern hemisphere for this period (O'Neill et al., 2012). Note that in Bal-  
3 sim, H<sub>2</sub>SO<sub>4</sub> mixing ratios in July are taken from the Sat-sim simulation.

4 The simulation presented hereafter accounts for the standard deviations of aerosol SADs observed  
5 from the balloon-borne STAC instrument and shown in **Figure 1**.

6

7

8

9

### 10 **3. Impact of the volcanic aerosols on stratospheric nitrogen compounds:** 11 **comparisons between balloon-borne observations and model simulations**

12

#### 13 **3.1 Impact of transport on simulated N<sub>2</sub>O and NO<sub>y</sub>**

14 It has been shown that wind fields from meteorological analysis produce an excessively strong  
15 Brewer-Dobson circulation (BDC) in the stratosphere (e.g. Legras et al., 2005; Monge-Sanz et al., 2007)  
16 which affects the ability of CTMs to represent the global distribution of long-lived tracers. Past model  
17 calculations used to significantly underestimate NO<sub>x</sub> and NO<sub>y</sub> concentrations (e.g. Sen et al., 1998; Gao  
18 et al., 1999; Wetzal et al., 2002; Stowasser et al., 2003) and Berthet et al., (2006) mainly attributed this  
19 problem to transport calculation issues for N<sub>2</sub>O. Following the work of Legras et al. (2005), REPROBUS  
20 has been driven by 3-hourly ECMWF wind fields obtained by interleaving operational analysis and  
21 forecasts. Using these more timely resolved and less noisy ECMWF wind fields reduced the ascent  
22 velocities of the upward branch of the Brewer-Dobson circulation in the tropics, largely reduced the  
23 model-measurement discrepancies by increasing the simulated global NO<sub>y</sub> and NO<sub>x</sub> amounts from  
24 increased N<sub>2</sub>O photo-oxidation (Berthet et al., 2006). In this configuration, the summer 2009  
25 REPROBUS simulations are in agreement with the SPIRALE in situ observations, especially at the  
26 altitudes of the Sarychev aerosols (**Figure 2**).

27 The effect on simulated total NO<sub>y</sub> can be investigated by converting the vertical profile of N<sub>2</sub>O,  
28 following the strategy of Berthet et al. (2006) based on N<sub>2</sub>O-NO<sub>y</sub> correlation curves. Since the study of  
29 Michelsen et al. (1998) global emissions of N<sub>2</sub>O have increased and therefore the N<sub>2</sub>O-NO<sub>y</sub> correlation  
30 curve reported therein needs some revision. As a consequence, we have constructed updated high-  
31 latitude N<sub>2</sub>O-NO<sub>y</sub> correlation curves from the IMK/IAA V5R\_220 MIPAS-Envisat data for the high-  
32 latitude in summer stratosphere (Fischer et al., 2008; data available at [http://www.imk-  
33 asf.kit.edu/english/308.php](http://www.imk-asf.kit.edu/english/308.php)) as shown in **Figure 3** in which the Michelsen et al.'s former results are also  
34 represented for comparison. The estimated vertical profile of NO<sub>y</sub> (hereafter NO<sub>y</sub>\*) derived from the  
35 conversion of the in-situ profile of N<sub>2</sub>O using the MIPAS correlation curve is presented in **Figure 2**.  
36 Above 25 km, the NO<sub>y</sub>\* profile presents a non-monotonous trend in comparison with the NO<sub>y</sub> profile  
37 computed by the 3D version of REPROBUS, since in the model the vertical structures on the observed  
38 N<sub>2</sub>O profile are amplified by the conversion to NO<sub>y</sub>\* through the N<sub>2</sub>O-NO<sub>y</sub> correlation. Above about 20  
39 km NO<sub>y</sub>\* is almost systematically lower than the 3D REPROBUS NO<sub>y</sub> profile whereas better overall  
40 agreement is observed for the volcanic aerosol loaded lower stratosphere.

41

42

#### 43 **3.2 Photochemical conditions**

44

45 N<sub>2</sub>O<sub>5</sub> is produced mainly at night from the recombination of NO<sub>2</sub> with NO<sub>3</sub> and destroyed during the  
46 day by photolysis leading to the reformation of NO<sub>2</sub>. NO<sub>3</sub> is formed mainly at night by the reaction of  
47 NO<sub>2</sub> with O<sub>3</sub>. The summer season provides particular conditions for stratospheric NO<sub>y</sub> chemistry. In this  
48 period, some regions of the polar stratosphere receive continuous solar illumination for many weeks  
49 which results in permanent photolysis reactions and enhances conversion of nitrogen reservoirs (N<sub>2</sub>O<sub>5</sub>  
50 and HNO<sub>3</sub>) to NO<sub>x</sub>. Decreases of HNO<sub>3</sub>, the major NO<sub>y</sub> species at mid- and high latitudes are manifest



1 in observations (Santee et al., 2004; Lindenmaier et al., 2011) and models (Chipperfield, 1999). With  
2 the onset of continuous photolysis in high-latitude air masses,  $N_2O_5$  production (occurring significantly  
3 at night) stops abruptly because  $NO_3$  amounts are kept low due to rapid photolysis, thereby preventing  
4  $N_2O_5$  formation as shown on **Figure 4** above the Esrange/Kiruna balloon launching base.  $N_2O_5$   
5 hydrolysis ceases as well and the  $NO_x/NO_y$  ratio becomes primarily controlled by gas-phase reactions,  
6  $NO_x$  being principally destroyed by  $NO_2 + OH$  reaction and produced by  $HNO_3 + OH$  reaction and  
7 photolysis of  $HNO_3$  (Osterman et al., 1999; Dufour et al., 2005). A period of enhanced conversion of  
8  $NO_y$  to  $NO_x$  occurs until about beginning of August (Brühl et al., 1998) as reflected in **Figure 4**.  
9 Consequently,  $NO_x$  becomes the principal catalyst for ozone loss with local destruction rates which can  
10 exceed 0.3% per day in summer air masses (Fahey and Ravishankara, 1999).

11 **Figure 4** shows the recovery of  $N_2O_5$  on the return of sunset at high latitude (around day 213 at the  
12 beginning of August for the considered location) around 17.5 km. When  $NO_3$  reforms at the beginning  
13 of August, significant conversion of  $NO_2$  to  $N_2O_5$  occurs during the night. The associated decrease in  
14  $NO_x$  is reflected in **Figure 4**. The conversion of  $N_2O_5$  to  $HNO_3$  through reaction (1) occurs almost  
15 exclusively at night. As the season progresses, the increase in the conversion rate caused by the increase  
16 in night duration is moderated by the decrease in  $NO_2$  amounts at the beginning of the night. As  
17 expected, increasing SAD values in the model to reproduce the volcanic aerosol levels has no effect on  
18  $N_2O_5$  (and on the production of  $HNO_3$ ) and on  $NO_x$  during the period of continuous solar illumination.  
19 However, from the onset of  $N_2O_5$  recovery a significant decrease in the  $N_2O_5$  and  $NO_x$  levels in  
20 comparison with the background aerosol simulation is calculated as the lifetime of  $N_2O_5$  in reaction (1)  
21 is reduced (e.g. Kinnison et al., 1994) and as further nitrogen oxides are converted to the more stable  
22  $HNO_3$  reservoir.

23 This situation implies that the balloon flights performed from August 7, 2009 match the  
24 photochemical conditions for which volcanic aerosols likely had an impact on  $NO_y$  partitioning via  
25 elevated  $N_2O_5$  hydrolysis. Some variability in modelled  $N_2O_5$  (**Figure 4**) is due to the effect of  
26 meridional transport to high latitudes which can be an important factor setting the stage of the chemical  
27 conditions at the measurements location.

28

29

### 30 3.3 $NO_2$

#### 31 3.3.1 Model comparisons with observations

32

33 In a stratosphere impacted by enhanced aerosol loadings after major volcanic eruptions,  $NO_x$  amounts  
34 are expected to be linked to aerosol concentrations. Observations of the  $NO_2$  column has shown strong  
35 anti-correlation with increasing aerosol amounts in mid-latitude conditions in spring (Mills et al., 1993).  
36 In polar summer, strong reductions of  $NO_x$  amounts have been observed in the presence of the Pinatubo  
37 aerosols as a result of enhanced  $N_2O_5$  hydrolysis (e.g. Solomon et al., 1994). For the Sarychev situation,  
38 minima in  $NO_2$  concentrations appear closely correlated with enhancements in aerosol amounts in the  
39 lower stratosphere (**Figure 5**). Thus the empirical evidence supports the view that  $NO_x$  chemistry is  
40 largely driven by heterogeneous processes even in the case of a moderate volcanic eruption. Here  
41 reductions in expected  $NO_2$  of up to a factor of  $\sim 2$  is seen for aerosol increases of  $\sim 3$  (with respect to  
42 the mean profiles). Conversely, layers with lower aerosol amounts, i.e. not affected by transport of the  
43 volcanic aerosols, show maximums in  $NO_2$  concentrations.

44 Model simulations have been conducted to provide further insight into the chemical impact of the  
45 volcanic aerosols on  $NO_x$  and  $NO_y$  partitioning and to compare with several balloon-borne observations.  
46 **Figure 6** presents the measured in-situ profiles of  $NO_2$  obtained for two different cases of photochemical  
47 conditions, i.e. for SPIRALE-07082009 around 02:15 UT, at  $\sim 87^\circ$  SZA, and SPIRALE-242009, around  
48 21:15 UT at a SZA of  $\sim 100^\circ$ , together with REPROBUS model outputs for altitudes below 20 km where  
49 the Sarychev aerosols were present. The reference simulations (i.e. without volcanic aerosols)  
50 significantly overestimate the  $NO_2$  observations with differences as large 56-57% (values with respect  
51 to the measured profile) between 14 and 19 km for SPIRALE-07082009 and SPIRALE-24082009  
52 (**Table 1**). The model results have also been assessed by the remote sensing observations from the  
53 SALOMON and DOAS instruments flown on 25 August and 7 September 2009 respectively. Non-  
54 volcanic model calculations show also discrepancies with solar occultation measurements in the lower



1 stratosphere (**Figure 7**), where the model overestimates measured NO<sub>2</sub> by 51% and 75% for the  
2 SALOMON flight on 25 August 2009 and the DOAS flight on 7 September 2009, respectively (**Table**  
3 **1**).

4 The embedded plots in **Figure 6** and **Figure 7** show the comparison above the Sarychev aerosol  
5 layer, i.e. for the whole range of altitudes observed by the instruments (up to ~35 km). Calculated NO<sub>2</sub>  
6 amounts overestimate the observations by 23% and 15% on average above 20 km for the SPIRALE-  
7 07082009 and SPIRALE-07082009 simulations, respectively. These values suggest that the model-  
8 measurement differences in the lower stratosphere may be only partly attributed to remaining  
9 uncertainties in calculations of transport. This issue is further investigated in section 3.6. Above 20 km  
10 the simulated profiles show good agreement with SALOMON and DOAS observations, except above  
11 30 km for the flight on 25 August 2009.

12 The Sat-sim simulations driven by the aerosol content inferred from OSIRIS satellite data show  
13 significant improvement in comparison with the non-volcanic calculations, the model outputs matching  
14 well the NO<sub>2</sub> observations with model-measurement differences of 5-7% (in absolute values) for all  
15 dates (**Table 1**). Likewise, the measured NO<sub>2</sub> profiles and the model results obtained from the Bal-sim  
16 constrained by a range of aerosol SADs observed by the STAC aerosol counter show good agreement  
17 with for instance average differences of 3±20% and -16±20% for the SPIRALE-07082009 and  
18 SPIRALE-24082009, respectively. It can be noted that the REPROBUS calculations do not reproduce  
19 some of the vertical structures detected by the SPIRALE instrument, i.e. between 17.5 and 19.5 km for  
20 SPIRALE-07082009 and at 17 km and 20.5 km for SPIRALE-24082009. This is likely due to vertical  
21 resolution of the model or inaccurate simulation of mixing effects in the CTM as already mentioned in  
22 previous studies showing this kind of comparisons (e.g. Berthet et al., 2006). We note also that all  
23 simulation results deviate from the lower altitude points in the SALOMON and DOAS profiles. Part of  
24 this discrepancy might be due to effects of possible concentration inhomogeneities along the lines of  
25 sight which are likely to induce biases in the retrieved profiles from remote sensing instruments  
26 especially in the lower stratosphere (Berthet et al., 2007).

27 Calculated differences between the volcanic-aerosol-constrained and the reference simulations  
28 provide an estimation of the chemical perturbation induced by the Sarychev aerosols. Considering  
29 together the results from OSIRIS and balloon-driven simulations, reductions in NO<sub>2</sub> mixing ratios  
30 between 31 and 47 % are simulated on average below 19 km (**Table 2**). The similar NO<sub>2</sub> reduction for  
31 SPIRALE-07082009 and SPIRALE-24082009 once again indicates that enhanced hydrolysis of N<sub>2</sub>O<sub>5</sub>  
32 onto volcanic aerosols is efficient even for conditions of incomplete recovery of N<sub>2</sub>O<sub>5</sub>. For a stratosphere  
33 affected by the Pinatubo aerosols, decreases ranging from 30 to 45% have been reported both in model  
34 calculations of NO<sub>2</sub> concentrations (Kinnison et al., 1994; Webster et al., 1994) and in the NO<sub>2</sub> columns  
35 (Johnston et al., 1992; Koike et al., 1993; Koike et al., 1994; Solomon et al., 1994). At a glance, the  
36 amplitude in the NO<sub>2</sub> reduction is therefore similar for both eruptions but it should be noted that results  
37 from these above-mentioned studies were provided for different latitudes, various seasons and  
38 correspond to wider altitude ranges as a result of the larger vertical extent of the Pinatubo aerosol cloud.

39

### 40 3.3.2 Saturation effect of NO<sub>x</sub> reduction

41

42 The reduction of NO<sub>x</sub> from the results described above is significant but also indicates some  
43 saturation through reaction 1 for the range of SAD observed for the Sarychev aerosols. The partitioning  
44 between NO<sub>x</sub> and NO<sub>y</sub> is expected to become insensitive to increases in aerosol SAD beyond a certain  
45 value when N<sub>2</sub>O<sub>5</sub> hydrolysis is the dominant sink for NO<sub>x</sub> because the nighttime formation of N<sub>2</sub>O<sub>5</sub> by  
46 reaction of NO<sub>2</sub> and NO<sub>3</sub> is quadratically dependent on NO<sub>x</sub>. This effect is reflected in **Figure 8**  
47 presenting the NO<sub>2</sub> amounts versus aerosol SAD as observed by the SPIRALE instrument and simulated  
48 by the REPROBUS CTM. NO<sub>2</sub> reduction shows a kind of asymptotic behaviour as the heterogeneous  
49 rate of reaction 1 becomes large with increasing aerosol SAD. In this case 82-88% of NO<sub>y</sub> are stored in  
50 HNO<sub>3</sub>. We must keep in mind that Figure 8 does not accurately demonstrate the saturation effect because  
51 our NO<sub>x</sub>-SAD curve has been constructed for a wide range of altitudes (i.e. with different NO<sub>y</sub> amounts  
52 and photochemistry) and not for a constant level. Observations obtained separately for different aerosol  
53 loadings but similar in terms of altitude levels and SZA would have been necessary to point out a clear  
54 asymptotic value, as a proof of the saturation effect. Nevertheless, our results indicate saturation for  
55 SAD values larger than about 4 μm<sup>2</sup>.cm<sup>-3</sup> which is reached on average for altitudes around 18 km. The





1 net reduction of  $\text{NO}_x$  reported for the Pinatubo aerosols tends to saturate at similar SAD values in the  
2 18-22 km range, as shown in the works of Fahey et al. (1993), Kondo et al. (1997) and Sen et al. (1998).

### 3.4 $\text{HNO}_3$

3  
4  
5 **Figure 9** compares the  $\text{HNO}_3$  profiles observed by the SPIRALE instrument and the simulations by  
6 the REPROBUS CTM for SPIRALE-07082009 and SPIRALE-24082009. We show here model outputs  
7 for total  $\text{HNO}_3$  (i.e. both in the gas phase and condensed), but note that because  $\text{HNO}_3$  is rapidly released  
8 into the gas phase, gaseous  $\text{HNO}_3$  would give the same results.

9  
10 In the lower stratosphere, the simulated reference profiles for  $\text{HNO}_3$  are mostly within the errors bars  
11 of the measurements (calculated model-measurement differences are of -3% and -4% below 19 km for  
12 SPIRALE-07082009 and SPIRALE-24082009, respectively as shown in **Table 1**) though some specific  
13 vertical structures are not reproduced by the model. The agreement is even good up to 35 km confirming  
14 that transport may not be a major issue in the comparisons.

15  
16 Results from the volcanic-aerosol simulations appear also within the measurement error bars  
17 (calculated model-measurement differences are between 6 and 8% for the Sat-sim results for SPIRALE-  
18 07082009 and SPIRALE-24082009, respectively as shown in **Table 1**). The production of  $\text{HNO}_3$  by  
19 heterogeneous chemistry generally appears less effective in the lower stratosphere than above 20 km  
20 when volcanic aerosols are present (see figure 3 of Webster, 1994; Plate 3 of Danilin et al., 1999).  
21 However, the production of  $\text{HNO}_3$  in the lower stratosphere is considered as significant for the Sarychev  
22 derived aerosols because the simulations including volcanic aerosols increase simulated  $\text{HNO}_3$  amounts  
23 by 9-11% below 19 km as indicated by the Sat-sim results (**Table 2**). Simulated reduced levels of  $\text{NO}_x$   
24 correspond to the produced additional amounts of  $\text{HNO}_3$ . For instance, the simulated  $\text{NO}_x$  decrease of -  
25 0.21 ppbv matches the +0.22 ppbv increase of  $\text{HNO}_3$  at 16 km for SPIRALE-07082009. Note that in  
26 this context, the role of the  $\text{NO}_2 + \text{OH}$  reaction with respect to  $\text{NO}_x$  conversion by enhanced  $\text{N}_2\text{O}_5$   
27 hydrolysis on the detailed partitioning between  $\text{NO}_x$  and  $\text{HNO}_3$  is not so clear (Coffey and Mankin,  
28 1993).

29 After the Pinatubo eruption, maximum  $\text{HNO}_3$  column increases of 30-40% were measured at mid-  
30 latitudes (Koike et al., 1994). When Pinatubo aerosol SADs had decreased to values comparable to the  
31 summer 2009 SADs around 16 km, i.e.  $7.5\text{-}9 \mu\text{m}^2\cdot\text{cm}^{-3}$  in fall 1993 (Berthet et al., 2002), the percent  
32 change in the  $\text{HNO}_3$  column had dropped below 20% (Koike et al., 1994; Rinsland et al., 2003). Overall,  
33 this reported effect is larger than in our observations indicating a more limited production of  
34 stratospheric  $\text{HNO}_3$  after the Sarychev eruption. However, quantifying the difference between both  
35 eruptions in term of chemical effects remains difficult as mentioned for  $\text{NO}_2$ . In particular, the observed  
36 signature of the Pinatubo-induced  $\text{HNO}_3$  enhancement was not limited to the lower stratosphere and was  
37 prevailing above the 420-465 K (~16-18 km) vertical range (Webster et al., 1994; Santee et al., 2004).

### 3.5 $\text{NO}_2/\text{HNO}_3$ ratio

38  
39  
40 The uncertainty in the simulated  $\text{NO}_y$  is expected to be minimized by considering the ratios of  
41 individual components of  $\text{NO}_y$  to total  $\text{NO}_y$ , as shown by Wetzal et al. (2002) for summer mid-latitude  
42 conditions. When no measurements of total  $\text{NO}_y$  are available, the  $\text{NO}_2/\text{HNO}_3$  ratio can be used as a  
43 good approximation to reduce the uncertainty in the model estimate of  $\text{NO}_y$  (e.g. Webster et al., 1994;  
44 Berthet et al., 2006). This is especially useful for SPIRALE-07082009 and SPIRALE-24082009 for  
45 which modelled  $\text{NO}_2$  and  $\text{HNO}_3$  amounts account for more than 92% of total  $\text{NO}_y$ .

46  
47 **Figure 10** presents the  $\text{NO}_2/\text{HNO}_3$  ratios observed by SPIRALE in comparison with the REPROBUS  
48 model simulations. The  $\text{NO}_2/\text{HNO}_3$  ratio in the lower stratosphere is typically 0.2 but the measurements  
49 indicate a smaller ratio. Under background aerosol loadings the observed low  $\text{NO}_2/\text{HNO}_3$  ratios are not  
50 matched by the reference simulation with the differences below 19 km being 62-63% for both flights  
51 (**Table 1**). A good agreement is obtained between both measurements and the model by including the  
52 Sarychev aerosols with absolute differences decreasing to  $3\pm 20\%$  and 1% for the Balloon-aero-sim and  
53 Satellite-aero-sim simulations, respectively, for SPIRALE-07082009. No clear improvement can be  
54 noticed from the model-measurement comparisons of the  $\text{NO}_2/\text{HNO}_3$  ratio and the both species (**Figures**  
55



1 **4 and 7).** Again this indicate that uncertainties in transport calculation are not the main explanation for  
2 the model-measurement discrepancy observed for the lower stratosphere.

3 The Sat-sim aerosol constrained simulations of the reduction in the  $\text{NO}_2/\text{HNO}_3$  ratio are 36% and  
4 44% for SPIRALE-07082009 and SPIRALE-24082009, respectively (**Table 2**). These ratios are similar  
5 to the Bal-sim outputs. For the Pinatubo aerosol loaded stratosphere, comparable reductions ranging  
6 from 20 to 45% have been reported both in the observed  $\text{NO}_2/\text{HNO}_3$  column ratios (Koike et al., 1994)  
7 and in model calculations (Webster et al. (1994).  
8  
9

### 10 **3.6 One-dimensional model calculations**

11 The measurement-model comparisons still show some discrepancies above 20 km. A way to discard  
12 a possible remaining effect of transport and further improve the modelling of total  $\text{NO}_y$  is to use  
13 constrained one-dimensional (1D) calculations (Dufour et al., 2005; Berthet et al., 2006). These may  
14 allow us to refine the quantification of the enhanced heterogeneous processes resulting from the  
15 Sarychev eruption. Following the strategy of Berthet et al. (2006), the 1D-REPROBUS initialization is  
16 constrained by available  $\text{N}_2\text{O}$  observations (here the profile measured by SPIRALE) and by the  
17 corresponding  $\text{NO}_y^*$  profile as illustrated in **Figure 2**.

18 The 1D reference simulation (Ref-sim 1D) is computed with background aerosol levels, while the  
19 Sarychev aerosol affected simulation is constrained with the mean aerosol profile measured during the  
20 balloon-borne observations (Bal-sim 1D). As a result of the  $\text{NO}_y^*$  input in the calculations, the Ref-sim  
21 1D simulations show very good agreement for  $\text{NO}_2$  and  $\text{HNO}_3$  (and consequently for  $\text{NO}_2/\text{HNO}_3$ ) with  
22 the SPIRALE measurements above 20 km, thus mostly leading to better results than the 3D reference  
23 simulation (**Figures 6, 9 and 10**) especially for  $\text{NO}_2$  and  $\text{NO}_2/\text{HNO}_3$ . At the altitudes affected by the  
24 Sarychev aerosols, the model results deviate from the observed profile. Here differences are 48-60%  
25 (absolute values) for the  $\text{NO}_2/\text{HNO}_3$  ratio for SPIRALE-07082009 and SPIRALE-24082009 (**Table 1**).  
26 We note that fine structures in the measured profile are not reproduced by the 1D model as a matter of  
27 height resolution and interpolation (Berthet et al., 2006). As for the 3D model profiles, the 1D  
28 simulations constrained by observed aerosol quantities (Bal-sim 1D) are in good agreement with the in  
29 situ measurements with the calculated model-observation differences being 12-16% (absolute values)  
30 for the  $\text{NO}_2/\text{HNO}_3$  ratio (**Table 1**). Overall the 1D simulations including volcanic aerosol loadings do  
31 not show evidence of significant improvement in the comparisons. These results confirm that the model-  
32 observations differences in the lower stratosphere can be mostly attributed to heterogeneous processes  
33 and not to spurious calculations of transport.

34 The calculated chemical impact of the Sarychev aerosols on  $\text{NO}_2$  and  $\text{HNO}_3$  gives percentage values  
35 comparable to the 3D simulation results, with for instance a reduction by 22 and 34% in  $\text{NO}_2$  amounts  
36 for SPIRALE-07082009 and SPIRALE-24082009, respectively (**Table 2**).  
37  
38  
39  
40  
41

## 42 **4. Impact of the volcanic aerosols on the coupled catalytic cycles involving** 43 **halogen, nitrogen and $\text{HO}_x$ compounds**

### 44 45 **4.1 Chlorine partitioning**

46 Several studies have revealed the impact of the Pinatubo eruption on the stratospheric halogen  
47 chemistry. This has been shown to be of particular importance regarding ozone destruction processes  
48 through the partitioning of chlorine reservoir species and activation of chlorine radicals on volcanic  
49 aerosols (e.g. Solomon, 1999 and references therein). Some volcanic eruptions are likely to inject  
50 halogenated compounds within the stratosphere therefore impacting directly the halogen content and  
51



1 bypassing (or adding to) in situ heterogeneous processes. For the Sarychev volcano eruption, an injection  
2 of several ppbv of HCl in the stratosphere has been reported by Carn et al. (2016) using Microwave  
3 Limb Sounder (MLS) data, mainly below the 140 hPa level (see their Figure 4). However the exact  
4 altitude of injection is inaccurate because of the low vertical resolution of MLS data, i.e. ~3 km. In  
5 addition, MLS HCl measurements are known to be biased high below the 100 hPa level and are not  
6 recommended for scientific use (Livesey et al., 2011) making difficult to infer a robust injection amount.  
7 HCl amounts in the lower stratosphere has returned to background levels within about two weeks (Carn  
8 et al., 2016). No difference with respect to background HCl levels is apparent above Kiruna and over  
9 the Northern hemisphere in July and at the period of the balloon campaign, indicating fast dilution of  
10 the HCl plume after the eruption (MLS data available at <http://giovanni.gsfc.nasa.gov/giovanni/> and  
11 <http://disc.sci.gsfc.nasa.gov/>). Thus no effect is expected on the total inorganic chlorine in our model  
12 calculations.

13 We therefore examine the direct impact of the Sarychev sulfate aerosols on the chlorine partitioning  
14 in connection with NO<sub>x</sub> and HO<sub>x</sub> in the lower stratosphere. Heterogeneous reactions on volcanic aerosols  
15 involving the ClONO<sub>2</sub> and HCl chlorine reservoirs (especially reaction 2) have been shown to play a  
16 major role in determining the abundance of active chlorine and therefore they are likely to compete with  
17 reaction 1 as a sink of NO<sub>x</sub> depending on ambient temperature values (e.g. Hanson et al., 1994).  
18 Significant decreases of HCl and corresponding increases in ClONO<sub>2</sub> have been reported for  
19 temperatures below 210 K in the lower stratosphere with a strong temperature sensitivity when volcanic  
20 aerosol amounts are large (Michelsen et al., 1999; Webster et al., 1998; Webster et al., 2000). **Table 3**  
21 presents the calculated effects of the Sarychev aerosols on the partitioning of the halogen species at 16.5  
22 km. Simulated levels of HCl decrease by 3% (~20 pptv) which is much smaller than the change observed  
23 by Webster et al. (2000) for the Pinatubo aerosols (about -31% at 21 km). Higher levels of ClONO<sub>2</sub> are  
24 simulated post the Sarychev eruption with respect to background conditions with increases of about 16%  
25 (~20 pptv). ClO and HOCl increase by 106% (~6 pptv) and 217% (~2 pptv) respectively at daytime. It  
26 is interesting to notice that these results for ClO are comparable to the calculations of Tie et al. (1994)  
27 who show ClO increases by at least 5 pptv in the lower stratosphere for summer 1992 at a time when  
28 Pinatubo related aerosol SADs were similar to August 2009 values.

29 The impact of the volcanic aerosols on the chlorine partitioning appears somewhat small since it is  
30 primarily the consequence of the increasing losses of HCl by enhanced OH through reaction HCl + OH  
31 → Cl + H<sub>2</sub>O (McElroy et al., 1992; Webster et al., 2000) rather than by reaction 2 for which the  
32 efficiency is low in the ~215-225 K range of temperatures mostly encountered in the lower stratosphere  
33 over the August-September 2009 period (see Figure 9 in Jégou et al., 2013). In fact, in the model HO<sub>x</sub>  
34 is increased by 51% (~1.4 pptv) (**Table 3**) and destruction of HCl by OH is faster than the HCl formation  
35 reaction Cl + CH<sub>4</sub> → HCl + CH<sub>3</sub>. An additional source of OH may be due to photolysis of HNO<sub>3</sub>  
36 (Rodriguez et al., 1991; Webster et al., 2000). Also the decreased reaction rate of reaction NO<sub>2</sub> + OH +  
37 M → HNO<sub>3</sub> + M in reduced NO<sub>x</sub> conditions (Kinnison et al., 1994) may increase OH. As also described  
38 by Bekki and Pyle (1994), subsequent production of reactive chlorine and increase in ClO is  
39 accompanied by an increase in ClONO<sub>2</sub> amounts through increased rate of reaction ClO + NO<sub>2</sub> + M →  
40 ClONO<sub>2</sub> + M, for which ClO is the limiting reactant. To a lesser extent, decreased rate of reaction 3 for  
41 the observed temperature range contributes to this increase. Overall, the ClONO<sub>2</sub> increase compensates  
42 for the HCl decrease in reaction 3 (Kinnison et al., 1994; Michelsen et al., 1999; Webster et al., 2000).  
43 HOCl amounts rise as a result of slightly enhanced ClONO<sub>2</sub> hydrolysis and production by enhanced  
44 HO<sub>x</sub> through reaction HO<sub>2</sub> + ClO → HOCl + O<sub>2</sub>.

45  
46

## 47 4.2 Bromine compounds

48

### 49 4.2.1 Effect on BrO

50 Coupling between chlorine and bromine compounds is of particular importance in the lower  
51 stratosphere and the role of bromine chemistry in regulating chlorine partitioning must be considered  
52 (e.g. Lary et al., 1996; Erle et al., 1998; Salawitch et al., 2005). Heterogeneous bromine reactions are



1 expected to increase the coupled gas phase ClO/BrO catalytic ozone destruction cycles. Because  
2 BrONO<sub>2</sub> hydrolysis (reaction 4) is not temperature dependent, its effects on the chemistry of the lower  
3 stratosphere are primarily dependent on the aerosol loading and not on latitude or SZA (Lary et al.,  
4 1996; Kondo et al., 1997; Erle et al., 1998).

5 Some incidents of a direct injection of bromine into the stratosphere by volcanic eruptions have been  
6 reported. The study of Hormann et al. (2013) based on space-borne observations of BrO however  
7 indicate that stratospheric injection of bromine was insignificant after the Sarychev eruption. We  
8 therefore expect that stratospheric bromine chemistry was only modified by the enhanced aerosol  
9 loading (e.g., Lary et al., 1996). BrO was the only key halogenated radical detected during the summer  
10 2009 balloon campaign. Vertical profiles were provided by the SALOMON and DOAS instruments on  
11 25 August 2009 and 7 September 2009 respectively (**Figure 11**). They were simultaneously measured  
12 with the NO<sub>2</sub> profiles presented in section 3.2.2. When volcanic aerosol SAD are included BrO amounts  
13 are increased in the lower stratosphere, matching the observations within the error bars (**Figure 11**).  
14 Differences between the model and the observations and between the various simulations are  
15 summarized in **Table 1** and **Table 2** respectively.

16 Simulated results related to the bromine chemistry at 16.5 km are presented in **Table 3** for the  
17 August-September 2009 period. At daytime part of the BrO enhancement is linked to the decreased loss  
18 by the three body reaction with decreased NO<sub>2</sub>. The other part is expected to be controlled by BrONO<sub>2</sub>  
19 hydrolysis which is by far the most efficient bromine heterogeneous reaction in the temperature range  
20 observed in our study (Hanson and Ravishankara, 1995; 1996). Under high aerosol loading the rate of  
21 the BrONO<sub>2</sub> hydrolysis is likely to compete with the BrONO<sub>2</sub> photolysis and with other gas phase  
22 reactions which normally control the bromine partitioning at daytime (Lary et al., 1996). Here note that  
23 the conclusion of Kreycey et al., (2013) on a possibly larger ratio of the photolysis and the three body  
24 formation reaction for BrONO<sub>2</sub>(J(k) than compiled by Sander et al., (2011) is not by affected by the  
25 presence of the Sarychev aerosols in the lower stratosphere, since they addressed solar occultation  
26 observations for solar zenith angles < 92.5° at 31 km (i.e., tangent heights > 24 km). After sunset  
27 BrONO<sub>2</sub> production is ceasing and its enhanced hydrolysis on volcanic aerosols leads to strongly  
28 increased formation of HOBr (+3.9 pptv or +141%) at an early stage of the night so that little BrONO<sub>2</sub>  
29 remains before dawn. This conversion at nighttime results in further release of OH and Br atoms in the  
30 morning through photolysis of HOBr.

31 However, it is not clear if BrONO<sub>2</sub> hydrolysis is mainly responsible for the increase in BrO within  
32 the lowermost stratosphere. Dedicated simulations to estimate the respective contribution of gas-phase  
33 chemistry and heterogeneous processes on the control of BrO production under volcanic conditions have  
34 thus been performed. The effects of the Sarychev aerosols on each chemical compound are calculated  
35 by switching off reaction 4 and compared in terms of percentage differences with the simulations  
36 including all chemistry. Results are summarized in **Table 3**. It particularly shows that under the  
37 Sarychev aerosol loading, 18% of the daytime BrO production (+0.9 pptv or +22% at 16.5 km during  
38 the August-September 2009 period when volcanic aerosols were present) is due to BrONO<sub>2</sub> hydrolysis.  
39 This results implies that bromine chemistry in the gas phase coupled to processes controlling the NO<sub>y</sub>  
40 partitioning mainly govern BrO amounts (e.g., Lary et al., 1996).

#### 41 42 **4.2.2 Role of BrONO<sub>2</sub> hydrolysis on other compounds**

43 As shown in **Table 3** for an altitude of 16.5 km, at night BrONO<sub>2</sub> amounts are mainly affected by  
44 reaction 4 which controls 98% of its decrease under volcanic aerosol influence. Nearly 100% of the  
45 night-time HOBr production is due to BrONO<sub>2</sub> hydrolysis which accounts for 44% of the increase in  
46 OH radical amounts from the subsequent photolysis of HOBr at dawn. Therefore, under volcanic  
47 conditions enhanced BrONO<sub>2</sub> hydrolysis nearly matches the contribution of nitrogen chemistry (see  
48 section 4.1) as a source of OH (e.g., Hanisco et al., 2001).

49 This additional release of OH radicals has significant consequences in the chemistry of the lower  
50 stratosphere. In our study the reduction in NO<sub>x</sub> from BrONO<sub>2</sub> hydrolysis are small (less than 2%) as  
51 well as the overall effects on nitrogen partitioning confirming the conclusions of Lary et al. (1996) and  
52 Kondo et al. (1997). In contrast, there is substantial repartitioning of the active chlorine families. The  
53 catalytic increase in OH due to the hydrolysis of BrONO<sub>2</sub> leads to a reduction in the HCl lifetime which  
54 is primarily dependent on the aerosol loading (Tie and Brasseur, 1996). The additionally produced OH



1 converts further HCl to ClO and, ultimately, to ClONO<sub>2</sub>. As shown in **Table 3**, ~60% of the HCl  
2 decrease, 39% of the ClO increase and 66% of the ClONO<sub>2</sub> increase are due to reaction 4 under the  
3 Sarychev aerosol loading, thus illustrating a significant enhancement of the coupling between the  
4 stratospheric chlorine and bromine photo-chemistry.

5  
6  
7  
8

## 9 **5. Stratospheric ozone**

10

### 11 **5.1 Chemical ozone change**

12

13 Several studies have demonstrated that the effect of the Pinatubo aerosols on stratospheric ozone  
14 depletion at mid-latitudes is particularly significant in winter and spring. For instance, maximum ozone  
15 losses of 20-30% were reported for the 12 and 22 km altitude range monitored at some mid-latitude  
16 locations during 1993 winter and spring (Hofmann et al., 1994) whereas O<sub>3</sub> decreases of 10-15%  
17 occurred for the total ozone column (McGee et al., 1994; Randel et al., 1995). For the mid-latitude total  
18 ozone column Tie and Brasseur (1995) calculated reductions of the order of 6% in late winter/early  
19 spring. Similar decreases of total ozone were simulated for the summer northern hemisphere by Brasseur  
20 and Granier (1992).

21 It is interesting to estimate the stratospheric ozone depletion induced by the Sarychev eruption which  
22 differs from the Pinatubo eruption in terms of aerosol loading, season and latitude of injection, and  
23 aerosol residence time. As said above, the model does not directly calculate possible effects of aerosols  
24 on stratospheric temperature and circulation. All our simulations use the same transport calculations,  
25 whereas ozone loss from Pinatubo in the northern mid-latitudes can be both attributed to chemical and  
26 transport (such as increased tropical upwelling) effects (e.g. Telford et al., 2009). In the following, we  
27 therefore solely calculate the change in ozone due to photochemistry.

28 We then compare model simulations with enhanced and background aerosol levels (**Figure 12**).  
29 Results indicate chemical reductions in ozone of a few percent following the eruption when aerosol  
30 levels are computed from the OSIRIS space-borne data. Accumulated ozone depletion reaches its  
31 maximum above Kiruna around mid-September with changes of -1.5% (-20 ppbv) and -2.5% (-25 ppbv)  
32 at 16.5 km and 14 km, respectively. Similar ozone changes are simulated when the model is driven by  
33 the lower values of aerosol loading taken from STAC in-situ observations whereas when maximum  
34 aerosol values from the STAC instrument are used ozone depletion is -2.8% (-25 ppbv) and -4% (-35  
35 ppbv) at 16.5 km and 14 km, respectively (not shown). We clearly see that the reduction increases with  
36 decreasing altitude. Ozone depletion values close to the tropopause appear larger than in the lower  
37 stratosphere. This conclusion must be taken cautiously because the model does not include detailed  
38 influence of various other chemicals (especially organic compounds) entrained from the troposphere  
39 into lower stratosphere.

40

41

### 42 **5.2 Chemical mechanisms for the ozone change in the lower stratosphere**

43

44 In the lower stratosphere ozone removal rates are mainly controlled by the HO<sub>x</sub> and halogen catalytic  
45 cycles which have been found to typically account for 30-50% and 30% of the total ozone loss  
46 respectively, in non-volcanic conditions (Portmann et al., 1999; Salawitch et al., 2005). The NO<sub>x</sub> cycles  
47 play a relatively minor role in the direct removal of ozone in the lower stratosphere but, as a result of  
48 the coupling among the NO<sub>x</sub>, HO<sub>x</sub> and halogen cycles, the rate of ozone removal is still very sensitive  
49 to the concentration of NO<sub>x</sub> (Wennberg et al., 1994; Gao et al., 1999; Portmann et al., 1999; Salawitch  
50 et al., 2005). Through the reaction of HO<sub>2</sub> with NO (HO<sub>2</sub> + NO → NO<sub>2</sub> + OH), the decreased NO<sub>x</sub>  
51 concentrations after the Sarychev eruption result in a larger HO<sub>2</sub>/OH ratio (as shown in **Table 3**) than  
52 for background conditions (HO<sub>2</sub>/OH ratios typically ranging from 4 to 7). Because the photochemical



1 removal of ozone in the lower stratosphere is dominated by processes involving HO<sub>2</sub>, catalytic ozone  
2 destruction by HO<sub>x</sub> cycles is likely to be amplified after volcanic eruptions (Wennberg et al., 1994;  
3 1995) though ozone loss rates are limited due to the saturation of the NO<sub>x</sub>/NO<sub>y</sub> response. After the  
4 eruption of Sarychev the effectiveness of halogen cycles is enhanced due to increased ClO<sub>x</sub> resulting  
5 from OH increase (**Table 3**) (as explained in section 4.1). As said above, heterogeneous reactions  
6 activating chlorine are strongly and non-linearly dependent on temperature, implying slow rates at the  
7 average mid-latitude temperature conditions (minimum values of 215 K) (Hanson et al., 1994; Webster  
8 et al., 1998; Michelsen et al., 1999). Under these conditions the simulated depletion in ozone is  
9 restrained similarly to the finding of Tie et al. (1994). Note that in their study ozone reduction was about  
10 5% in the lower summer stratosphere when Pinatubo aerosol SADs were comparable to our  
11 observations.

12 Part of the ozone depletion can be related to the coupled BrO<sub>x</sub>/ClO<sub>x</sub> cycle which is expected to be  
13 responsible for 20-25% of the halogen-controlled loss under non-volcanic aerosol conditions (Portmann  
14 et al., 1999; Salawitch et al., 2005). **Table 3** shows that the hydrolysis of BrONO<sub>2</sub> accounts for more  
15 than 22% of the ozone loss at 16.5 km after the Sarychev eruption. Reaction 4 acts as a source of OH  
16 and accordingly reduces the HCl lifetime. This reduction in HCl lifetime is accompanied by an increase  
17 in the ClO<sub>x</sub> concentration and thereby indirectly couples the atmospheric chemistry of chlorine and  
18 bromine to amplify the chlorine-mediated ozone depletion. Because the sticking coefficient for  
19 hydrolysis of BrONO<sub>2</sub> on sulfate aerosols is not temperature dependent, this effect occurs at all latitudes  
20 and seasons in the lower stratosphere during high aerosol loading periods (Lary et al., 1996; Tie and  
21 Brasseur, 1996).

22  
23  
24  
25

## 26 6. Summary and conclusions

27

28 Our study provides key observations of the chemical perturbation in the lower stratosphere by the  
29 moderate Sarychev volcano eruption in June 2009. 3D and 1D CTM simulations are performed to  
30 interpret balloon-borne observations of some key chemical species made in the summer high-latitude  
31 lower stratosphere. The modelled chemical response to the volcanic aerosols is treated by comparing  
32 simulations using background aerosol levels and simulations driven by volcanic aerosol amounts  
33 inferred from balloon-borne and space-borne observations.

34 Quantifying the impact of volcanic aerosols on stratospheric ozone chemistry is difficult as chemical  
35 and dynamical (radiative) effects simultaneously occur (Pitari and Rizi, 1993; Robock, 2000). The  
36 model is a CTM driven by ECMWF off-line meteorological data and does not describe radiative  
37 processes. In other words, volcanic aerosol radiative effects are not directly interactive with the  
38 circulation computed by the model. Radiative processes from the injection of volcanic aerosols in the  
39 tropics have been shown to have an impact on mean meridional circulation and ozone transport  
40 (Brasseur and Granier, 1992; Pitari et Rizi, 1993). In our study, effects of the Sarychev aerosols on mid-  
41 latitude stratospheric dynamics, if any, are at least at the first order intrinsically taken into account in  
42 the ECMWF analyses used for all simulations. REPROBUS does not take into account the aerosol  
43 impact on calculated photolysis rates which is likely to result in some differences between models when  
44 this process is computed or ignored (Pitari et Rizi, 1993; Pitari et al., 2014). However because the  
45 Sarychev eruption has impacted only mid-latitude lower stratosphere the effect on the photolysis  
46 frequency of molecular oxygen and ozone due to absorption and backscattering of solar radiation by the  
47 volcanic aerosols is expected to be very small in this region (Tie et al., 1994). Therefore, since all our  
48 simulations have been driven with the same wind and temperature fields our approach only estimates  
49 the chemical effects of the Sarychev aerosols.

50 The NO<sub>y</sub> chemistry appears to be very sensitive to the increase in SAD within the lower stratosphere  
51 resulting from the Sarychev eruption. A decrease in the NO<sub>x</sub> abundances is evident but shows some  
52 saturation as emphasized in a number of studies referring to cases of high sulfate aerosol loadings (e.g.  
53 Fahey et al., 1993). The effect of volcanic aerosols on nitrogen partitioning is also reflected in the



1 calculated production of  $\text{HNO}_3$  as a result of the decrease of the  $\text{N}_2\text{O}_5$  nitrogen reservoir from its  
2 enhanced hydrolysis and  $\text{NO}_x$  reduction.

3 Although direct comparisons in terms of solar illumination, latitude, injection altitudes and  
4 temperature are not possible for distinct volcanic eruptions such as Pinatubo and Sarychev, it is  
5 interesting to compare the effect of both eruptions on the photochemistry of the lower stratosphere.  
6 Overall, although different in magnitude, the eruptions of Pinatubo and Sarychev show similar observed  
7 and simulated depletion of  $\text{NO}_2$ , probably due to the saturation effect of the enhanced  $\text{N}_2\text{O}_5$  hydrolysis.  
8 In comparison with the Pinatubo period, the Sarychev aerosols led to less overall  $\text{HNO}_3$  production in  
9 the stratosphere possibly because the related  $\text{HNO}_3$  enhancement has been shown to be considerably  
10 weaker in the lowermost stratosphere (below  $\sim 18$  km) than for sulfur injection into higher altitudes  
11 (Webster et al., 1994; Santee et al., 2004). However, one must notice that previously reported modelling  
12 studies on the Pinatubo aerosols were conducted with former chemical kinetic rate constants and  
13 photolysis rates which have been largely updated ever since, somewhat adding complexity for  
14 comparisons discussed within the present study.

15 For the Pinatubo aerosols, ozone destruction was not observed throughout the volcanic aerosol layer  
16 because  $\text{N}_2\text{O}_5$  hydrolysis reduced  $\text{NO}_x$  related ozone loss, which even resulted in small increases of  
17 ozone in the middle stratosphere (Bekki and Pyle, 1994; Tie and Brasseur, 1995). For the Sarychev  
18 eruption, the volcanic aerosol layer is restrained to altitude levels below 19 km where the ozone  
19 destruction processes by  $\text{HO}_x$  and halogen catalytic cycles are expected to play a major role (e.g.  
20 Salawitch et al., 2005) with some sensitivity towards  $\text{NO}_x$  levels. To summarize, the increased  
21 production of  $\text{HNO}_3$  via  $\text{N}_2\text{O}_5$  hydrolysis enhances the photolytic production of OH from  $\text{HNO}_3$ . As a  
22 result, the gas-phase sink for HCl by reaction with OH is slightly enhanced and is associated with an  
23 increase of ClO amounts. An important result from the heterogeneous hydrolysis of  $\text{BrONO}_2$  is the  
24 formation and subsequent photolysis of additional HOBr. The OH so produced additionally converts  
25 HCl to ClO (and ultimately to  $\text{ClONO}_2$ ). Accordingly, there is substantial repartitioning of the active  
26 chlorine but effects of the  $\text{BrONO}_2$  hydrolysis on nitrogen partitioning are insignificant. In this chemical  
27 context, the magnitude of the ozone response to the Sarychev volcanic perturbation appears limited (i.e.  
28 between -2.5 and -4% at 14 km considering the whole range of observed SADs) because the saturation  
29 of the  $\text{NO}_x/\text{NO}_y$  response limits the increase in  $\text{HO}_x$  and in active chlorine (ClO) by enhanced  $\text{HO}_x$ ,  
30 precluding important ozone loss rates. Moreover, stratospheric temperatures remained too high (i.e.  
31 mainly above 215 K) for efficient heterogeneous conversion of  $\text{ClONO}_2$  to active chlorine, which could  
32 have led to significant ozone depletion. For these temperature conditions, reaction 2 is not expected to  
33 compete with  $\text{N}_2\text{O}_5$  hydrolysis in the  $\text{NO}_y$  partitioning (Fahey et al., 1993; Cox et al., 1994). Eventually,  
34 the largest ozone destruction is restricted to the lowermost stratosphere (the bottom of the volcanic  
35 aerosol layer close to the tropopause) where catalytic cycles are primarily controlled by  $\text{HO}_x$  and where  
36 the  $\text{NO}_x$  photochemistry plays a very minor role.

37 However limitations in our model simulations also contribute to some model-measurement  
38 discrepancies. A first major difficulty is to drive the model simulations with representative and  
39 consistent inputs in term of volcanic aerosol loading. To address this issue, two different model runs for  
40 aerosol forcing have been performed, one using OSIRIS satellite data converted to aerosol SAD fields  
41 and the other one from in-situ balloon-borne observations. The OSIRIS satellite data represent zonally  
42 and daily averaged values of SAD which may vary from a 3D construction based on the local surface  
43 areas. The possible presence of aerosol streamers (geographical variations of the aerosol content)  
44 resulting from the transport of the volcanic aerosols over the northern hemisphere present from mid-  
45 July to September 2009 is likely to affect locally and regionally the  $\text{N}_2\text{O}_5$  abundances and, to a lesser  
46 extent,  $\text{NO}_2$  and  $\text{HNO}_3$  (Küll et al., 2002; Jucks et al. 1999). If our aerosol SAD dataset had been obtained  
47 when the local concentrations were higher than the zonal mean values, then the calculated rate of the  
48 heterogeneous reactions would be biased low and calculated  $\text{NO}_x$  and  $\text{HNO}_3$  abundances would be  
49 systematically biased high and low respectively. This is not however evident in all our comparisons  
50 from simulations based on OSIRIS aerosols. We also note that former studies mostly used 2D  
51 simulations to investigate the chemical effects of the enhanced aerosol burden following the Pinatubo  
52 eruption with some limitations in terms of meridional transport simulations. The second type of aerosol-  
53 constrained simulation uses SADs from balloon-borne observed profiles. By definition, such in situ  
54 observations deal with a particular location. Extrapolating in situ derived SADs to drive a 3D model at  
55 a large scale may induce inaccurate simulations of the chemical impact of the aerosols (Kondo et al.,



1 2000). To account for this SAD-related uncertainty, our simulations based on in-situ data encompass  
2 the range of SADs derived from the STAC balloon-borne observations over the August-September 2009  
3 period. Both satellite- and balloon-driven simulations give similar results in terms of  $\text{NO}_2$  and  $\text{HNO}_3$   
4 amounts possibly because the in-situ observations represent well the aerosol loading at the northern mid-  
5 latitudes. Another explanation is that the saturation effect (roughly when SADs become larger than 3  
6  $\mu\text{m}^2\cdot\text{cm}^{-3}$ ) of the  $\text{NO}_x/\text{NO}_y$  ratio is more relevant for the range of observed SADs than spatiotemporal  
7 inhomogeneities.

8 Secondly, adequate modelling of transport is also crucial for the partitioning of  $\text{NO}_y$ . Processes that  
9 control the vertical profiles of  $\text{NO}_2$  and  $\text{HNO}_3$  in the stratosphere are based on a complex interplay  
10 between dynamics and chemistry with the key issue to accurately simulate total  $\text{NO}_y$  which may be not  
11 systematically achieved with 3D CTM calculations. Improved simulations of transport can be obtained  
12 by combing operational analyses with forecasts to construct 3-hourly meteorological data to drive the  
13 CTM (Berthet et al., 2006). We have applied this strategy in the present study. Using 1D modelling  
14 driven by in-situ observations or calculating  $\text{NO}_2/\text{HNO}_3$  ratios to reduce transport effects does not  
15 clearly improve the model-measurement comparisons for the lower stratosphere. Although some  
16 features in the vertical profiles are not systematically captured by the model, this tends to indicate that  
17 the error in calculated transport is not large enough to account for the overall difference between  
18 measured and modelled  $\text{NO}_2$  and  $\text{HNO}_3$  when no volcanic aerosol loading is included in the model.  
19 Rather, these results show some evidence of the role of heterogeneous reactions at the surface of volcanic  
20 aerosols.

21 Thirdly, part of the discrepancies between model and observations might be attributed to spatial  
22 resolution issues. It may be tricky to compare model calculations with high resolution in-situ profiles  
23 and with remote sensing observations integrating over tens of kilometers (Berthet et al., 2007). For  
24 instance, discrepancies between remote sensing observations and model calculations have been reported  
25 for stratospheric  $\text{NO}_3$  in case of localized temperature inhomogeneities as a result of the strong  
26 dependence of  $\text{NO}_3$  cross sections and kinetics on temperature (Renard et al., 2001).  $\text{N}_2\text{O}_5$  and  $\text{NO}_2$  may  
27 be subsequently impacted because  $\text{NO}_3$ , together with  $\text{NO}_2$ , plays a central role in the equilibrium  
28 reaction controlling  $\text{N}_2\text{O}_5$  in the gas phase.

29 In our study, no comprehensive sulfur chemistry is included in the model. We have also excluded  
30 dynamical and radiative effects on the ozone response which have been shown to be of primary  
31 importance when dense volcanic clouds are present (e.g. Pitari and Rizi, 1993; Kinnison et al., 1994;  
32 Tie et al., 1994). In a forthcoming study it would be interesting to compare dynamical/radiative and  
33 chemical effects of moderate volcanic eruptions on stratospheric ozone using Chemistry-Climate models  
34 with full sulfur chemistry and aerosol-dynamics interactive calculations.

35 Finally, it might interesting to investigate the effects of other volcanic plumes coming from moderate  
36 volcanic eruptions which are then transported to high-latitude regions when stratospheric temperatures  
37 are more favourable for chlorine activation and enhanced ozone loss (e.g. in winter). Activation of  
38 chlorine from volcanic sulfate aerosols and associated ozone depletion is arguably more significant in  
39 the cold temperature conditions of winter/spring, even above the formation threshold of Polar  
40 Stratospheric Clouds (Hanson et al., 1994). The eruption of the Calbuco volcano in the southern  
41 hemisphere in April 2015 could be a good candidate for the study of this process.

42

43

44





1 **Acknowledgements.**

2 The authors are grateful to the CNES (French acronym for “Centre National d’Etudes Spatiales”)  
3 balloon launching team for successful operations and the Swedish Space Corporation at Esrange. The  
4 STRAPOLETE project and the associated balloon campaign has been funded by the French “Agence  
5 Nationale de la Recherche” (ANR-BLAN08-1-31627), CNES, and the “Institut Polaire Paul-Emile  
6 Victor” (IPEV). The study is supported by the French Labex « Étude des géofluides et des VOLatils–  
7 Terre, Atmosphère et Interfaces - Ressources et Environnement (VOLTAIRE) (ANR-10-LABX-100-  
8 01) managed by the University of Orleans. The ETHER database (CNES-INSU/CNRS) is partner of the  
9 project. Further support for the DOAS balloon measurements came through the Deutsche  
10 Forschungsgemeinschaft, DFG (grants PF-384/5-1 and 384/5-1 and PF384/9-1/2), and the European  
11 projects EU projects Reconcile (FP7-ENV-2008-1-226365) and SHIVA (FP7-ENV-2007-1-226224).  
12 We thank Michel Van Roozendael and Caroline Fayt from BIRA/IASB in Belgium for making available  
13 the WINDOAS algorithm very well-adapted for data reduction methods based on the Differential  
14 Optical Absorption Technique. We acknowledge the MIPAS/Envisat team from Karlsruhe Institute of  
15 Technology (KIT) for making IMK/IAA data available.

16

17



## 1 **Appendix A: Technical description**

### 2 **A.1 The STAC aerosol counter**

3  
4  
5 Aerosol size distributions are provided in the 0.4–5  $\mu\text{m}$  diameter size range (Ovarlez and Ovarlez,  
6 1995; Renard et al., 2008). Since 2008, the number of available size classes has been increased from 7  
7 to 14 within this size range (Renard et al., 2010). The counting uncertainty is obtained from the statistical  
8 probability given by Poisson counting statistics (Willeke and Liu, 1976). This uncertainty, defined as  
9 the relative standard deviation, is 60% for aerosol concentrations of  $10^{-3} \text{ cm}^{-3}$ , 20% for  $10^{-2} \text{ cm}^{-3}$ , and  
10 6% for concentrations higher than  $10^{-1} \text{ cm}^{-3}$ . Laboratory comparisons between two copies of the STAC  
11 aerosol counter using identical aerosol samples have shown differences of  $\pm 10\%$  for concentrations  
12 higher than  $10^{-2} \text{ cm}^{-3}$ . From these results, we define a measurement precision limited to  $\pm 10\%$ . It should  
13 be noted that comparisons with the aerosol concentrations measured by the University of Wyoming  
14 optical particle counter (Deshler et al., 2003) have shown consistent results between both instruments  
15 (Renard et al., 2002). STAC is calibrated in order to provide size distributions of non-absorbing liquid  
16 aerosols which have been unambiguously observed in the 8–19 km altitude range in the case of the  
17 Sarychev eruption (Jégou et al., 2013). Aerosol distribution moments are derived using well-known  
18 analytical expressions. Using a statistical approach as described in Deshler et al. (2003), STAC counting  
19 uncertainties (Poisson statistics and the  $\pm 10\%$  precision) translate into uncertainties on distribution  
20 moments, with estimated values of 40% for SAD. Profiles are typically averaged over a vertical range  
21 of 250 m (corresponding to  $\sim 1$  minute of measurements).

### 22 **A.2 The SPIRALE in-situ infrared spectrometer**

23  
24  
25 A detailed description of the instrumental characteristics of SPIRALE and of its operating mode can  
26 be found in Moreau et al. (2005). Six tunable laser diodes emitting in spectral micro-windows ( $< 1 \text{ cm}^{-1}$   
27  $^1$ ) in the mid-infrared domain (1250 to  $3000 \text{ cm}^{-1}$ ) are used for in situ measurements of trace gas species  
28 from the upper troposphere to the stratosphere. The six laser beams are injected into a multipass Herriott  
29 cell, comprising two mirrors spaced 3.50 m apart by a telescopic mast, allowing for 434.0 m optical  
30 path. This cell is deployed under the gondola during the flight, above  $\sim 9$  km altitude, i.e. when pressure  
31 is below  $\sim 300$  hPa and thus absorption lines are significantly narrower than the scanned micro-windows.  
32 Species concentrations are retrieved from direct absorption, by fitting experimental spectra with spectra  
33 calculated using HITRAN 2012 database (Rothman et al., 2013) and the temperature and pressure  
34 measured on board the gondola. Measurements of pressure (by two calibrated and temperature-regulated  
35 capacitance manometers) and temperature (by two probes made of resistive platinum wire) allow for  
36 conversion of the species concentrations to volume mixing ratios. Uncertainties on these parameters are  
37 negligible regarding the other uncertainties discussed below. The instrument provides measurements  
38 each 1.1 s, thus with a vertical resolution of a few meters depending on the vertical velocity of the  
39 balloon (2 to  $5 \text{ m s}^{-1}$ ). Absorption lines in the micro-windows  $1260.95\text{-}1261.25 \text{ cm}^{-1}$ ,  $1598.45\text{-}1598.85$   
40  $\text{cm}^{-1}$  and  $1701.50\text{-}1701.80 \text{ cm}^{-1}$  were selected for  $\text{N}_2\text{O}$ ,  $\text{NO}_2$  and  $\text{HNO}_3$ , respectively. The overall  
41 uncertainties for the volume mixing ratios have been assessed by taking into account the random errors  
42 and the systematic errors, and combining them as the square root of their quadratic sum (Moreau et al.,  
43 2005). There are two important sources of random errors: (1) the fluctuations of the laser background  
44 emission signal and (2) the signal-to-noise ratio. These error sources are the main contributions for  $\text{NO}_2$   
45 giving a total uncertainty of 30% at the lower altitudes (around 15 km), gradually reduced to 20% around  
46 20 km, and decreasing to 5% at higher altitudes (above 30 km). For  $\text{HNO}_3$  these random errors are less  
47 significant but two sources of systematic errors have to be considered: the laser line width (an intrinsic  
48 characteristic of the laser diode) and the non-linearity of the detectors resulting in an uncertainty of 20%  
49 on the whole profile. Concerning  $\text{N}_2\text{O}$  and ozone, which are abundant and measured using detection  
50 systems with proper linearity of the photovoltaic conversion, the overall uncertainties are 3% over the  
51 whole vertical profile, and decrease from 10% at 14 km (i.e. for mixing ratios below 1 ppmv) to 5%  
52 above 17 km, respectively. With respect to the above errors, systematic errors on spectroscopic data  
53 (essentially molecular line strength and pressure broadening coefficients) are considered to be negligible  
54 for these well studied species (Rothman et al., 2013). SPIRALE has been used routinely during the



1 2000's, in particular as part of European projects and satellite validation campaigns (Grossel et al., 2010;  
2 Mébarki et al., 2010; Krysztofiak et al., 2012 and 2015, and references therein).

3

### 4 **A.3 The DOAS remote-sensing UV-visible spectrometer**

5

6 Direct solar spectra from two UV/visible DOAS spectrometers are collected onboard the azimuth-  
7 controlled LPMA/DOAS (Limb Profile Monitor of the Atmosphere/Differential Optical Absorption  
8 Spectroscopy) balloon payload which carries a sun-tracker (Hawat et al., 1995). The solar reference  
9 spectrum is usually the spectrum for which the air mass along the line-of-sight and the residual trace gas  
10 absorption are minimal. The residual absorption in the solar reference is determined using Langley's  
11 extrapolation to zero air mass. Rayleigh and Mie scattering are accounted for by including a third order  
12 polynomial in the fitting procedure. The relative wavelength alignment of the absorption cross sections  
13 and the solar reference spectrum is fixed and only the measured spectrum is allowed to shift and stretch.  
14 O<sub>3</sub> Slant Column Densities (SCDs) are retrieved from the differential structures in the Chappuis  
15 absorption band between 545 nm and 615 nm. The line-of-sight absorptions of NO<sub>2</sub> are inferred from  
16 the 435 nm to 485 nm wavelength range. Two O<sub>3</sub> absorption cross sections recorded in the laboratory  
17 at 230K and 244 K, aligned to cross sections from Voigt et al. (2001), are orthogonalized and fitted  
18 simultaneously. Broad band spectral features are represented by a fourth order polynomial. Additional  
19 complications arise from the temperature dependence of the NO<sub>2</sub> absorption cross section (Pfeilsticker  
20 et al., 1999). The NO<sub>2</sub> analysis is performed using absorption cross sections recorded in the laboratory,  
21 scaled and aligned to convolved and orthogonalized cross sections from Harder et al. (1997) taken at  
22 217 K, and 230 K. The error bars of the retrieved SCDs are estimated via Gaussian error propagation  
23 mainly from the statistical error given by the fitting routine, the error in determining the residual  
24 absorber amount in the solar reference spectrum and the errors of the absorption cross sections. In total,  
25 typical accuracies of the DOAS O<sub>3</sub> and NO<sub>2</sub> measurements are better than 5% and 10%, respectively.  
26 The retrieval process for NO<sub>2</sub> is described in Butz et al. (2006).

27 Bromine monoxide (BrO) is detected in the UV wavelength range from 346 nm to 360 nm as  
28 recommended by Aliwell et al. (2002). This wavelength range contains the UV vibration absorption  
29 bands (4-0 at 354.7 nm, and 5-0 at 348.8 nm) of the A(<sup>2</sup>π) ← X(<sup>2</sup>π) electronic transition of BrO. Typical  
30 optical densities are 10<sup>-4</sup>–10<sup>-3</sup> for UV vibration absorption bands. The set of reference spectra used  
31 contains a NO<sub>2</sub> reference spectrum for T=233 K, and two O<sub>3</sub> spectra at T=197 K and T=253 K, in order  
32 to account for temperature effects. All NO<sub>2</sub> and O<sub>3</sub> spectra were recorded with the balloon spectrograph  
33 in the laboratory. The BrO reference is the absolute cross-section measured by Wahner et al. (1988),  
34 with the wavelength calibration taken from our own laboratory measurements. Profile information was  
35 obtained by a least-squares profile inversion technique (Maximum A Posteriori) (Rodgers, 2000).  
36 Further details on the BrO DOAS-retrieval and the profile inversion can be found in Harder et al. (1998)  
37 and (2000), Aliwell et al. (2002), Dorf et al. (2006b) and Kreygy et al. (2013).

38 In our study we use the DOAS profile recorded in the stratosphere during the balloon ascent on 7  
39 September 2009 between 15:15 UT (17:15 local time) and 16:35 UT (18:35 local time), corresponding  
40 to altitudes of 10 km and 30 km respectively.

41

### 42 **A.4 The SALOMON remote-sensing UV-visible spectrometer**

43

44 The data presented in this study were obtained using a SAOZ-type UV-visible spectrometer  
45 (Pommereau and Piquard, 1994) connected to a sun/moon tracker for the detection of ozone and NO<sub>2</sub>  
46 amounts. The one-band spectral window of SALOMON between 400 and 950 nm is adequate for the  
47 retrieval of absorption features over large spectral ranges, i.e. roughly from 400 to 680 nm for ozone  
48 and from 400 to 550 nm for NO<sub>2</sub>. The spectrum recorded at float altitude (more than 36.5 km)  
49 corresponds to a minimum air mass and is considered as a reference spectrum. Occultation spectra  
50 recorded for elevation angles between 0° and -5° below the gondola horizon are taken into account for  
51 the retrieval of the SCDs. Owing to the thermal insulation of the spectrometer, no spectral drift of the  
52 Fraunhofer lines and no instrumental resolution changes have been observed between the reference and  
53 the occultation spectra. The Rayleigh scattering contribution is calculated and removed from the spectra  
54 using these profiles and the spectral cross-sections given by Bucholtz (1995). Then, O<sub>3</sub> and NO<sub>2</sub> SCDs  
55 are determined by least-squares fits using the University of Bremen high resolution absorption cross-



1 sections convolved to the spectral resolution of the instrument (data available from <http://www.iup.uni-bremen.de/gruppen/molspec/databases/index.html>). Aerosols are a major low frequency spectral contribution which is removed by a high-pass filter to derive the NO<sub>2</sub> SCDs. All lines of sight are not used to derive SCDs since the retrieval is performed only when signal-to-noise ratios (computed in our case by the ratio of the fit maximum amplitude to the standard deviation between the measurement and the fit) are greater than 1. NO<sub>2</sub> fitting errors are typically of 5-9% for SCDs crossing the altitude levels of the volcanic aerosol layer (i.e. below ~19 km). Vertical concentration profiles have been derived using an a posteriori least-squares inversion technique (Rodgers et al., 2000) taking into account the fitting error and the uncertainties of the cross sections. Note that the data reduction method used in this study is described by Renard et al. (2000) and Berthet et al. (2002).

11 For the flight presented in this study we have added a HR4000 UV spectrometer from Ocean Optics to detect BrO absorption lines in the 346-360 nm range as done for the DOAS instrument. The spectrometer is thermally insulated and regulated using Peltier devices to avoid spectral shifts. It has its own connection to the sun tracker but collects the sunlight simultaneously with a Jobin-Yvon UV-visible spectrometer. We use the same data reduction method as for DOAS as described in details by Dorf et al. (2006b) to retrieve SCDs and the vertical profile of BrO. In our case the Wahner et al. BrO and Bremen ozone and NO<sub>2</sub> cross sections are convolved to the resolution of the instrument determined in the laboratory using a UV lamp. SCD data are smoothed to increase the signal-to-noise ratio. The altitude grid for profile inversion is 2 km. Associated random errors are those provided by the spectral fit. The major systematic error comes from the uncertain estimation of the residual BrO column above float altitude.

22  
23  
24

## 25 Appendix B: Model description

26

27 The REPROBUS 3D CTM computes the evolution of 55 species by means of about 160 photolytic gas-phase and heterogeneous reactions, with a time step of 15 minutes in this study. A semi-Lagrangian code transports 40 species or chemical families, typically long-lived tracers but also more unstable compounds (Lefèvre et al., 1994; Lefèvre et al., 1998).

31 Temperature, winds and surface pressure are specified from the 3D European Centre for Medium-Range Weather Forecast (ECMWF) meteorological data from the surface up to 0.01 hPa (i.e. about 80 km in altitude) on 91 levels. This results in a vertical resolution of about 0.45 km in the lower stratosphere. REPROBUS is driven by 3-hourly ECMWF wind fields obtained by interleaving operational analysis and forecasts because in this way spurious calculation of transport is reduced in comparison with simulations based on 6-hourly analysis (Legras et al., 2005; Berthet et al., 2006).

37 Gas-phase kinetics parameters used in the present study are based on the recommendation by the Jet-Propulsion-Laboratory (JPL) described in Sander et al. (2011). In particular for nitrogen gas-phase chemistry, revised kinetic data were recommended because, following a number of studies (e.g. Brown et al., 1999; Gao et al., 1999; Jucks et al., 1999; Osterman et al., 1999; Kondo et al., 2000; Prasad, 2003), a lower rate for the reaction of NO<sub>2</sub> with OH and a higher rate for HNO<sub>3</sub> with OH significantly reduced model-measurement discrepancies highlighted in former published work (e.g. Fahey et al., 1993; Kondo et al., 1997; Sen et al., 1998).

44 The heterogeneous chemistry module includes reactions on liquid aerosols. An analytical expression is used to calculate the equilibrium composition and volume of the H<sub>2</sub>SO<sub>4</sub>-H<sub>2</sub>O droplets as a function of temperature and the total amounts of H<sub>2</sub>O and H<sub>2</sub>SO<sub>4</sub> (Carslaw et al., 1995). The routine calculates the aqueous phase concentrations for the soluble species HCl, HBr, HOCl, and HOBr to calculate the rates of the heterogeneous reactions involving these compounds on stratospheric liquid aerosols. Reactions of N<sub>2</sub>O<sub>5</sub>, ClONO<sub>2</sub>, and BrONO<sub>2</sub> on/in sulfuric acid are usually dependent on the species' Henry's law solubility and liquid phase diffusion coefficient in the liquid as well as the surface and/or liquid phase reaction rates (Hanson et al., 1994; Shi et al., 2001; Sander et al., 2011). N<sub>2</sub>O<sub>5</sub> hydrolysis takes place at the surface of the particles (Hanson et al., 1994). As in a number of previous studies (e.g. Mills et al., 1993; Gao et al., 1999; Bracher et al., 2005) REPROBUS computes a  $\gamma$  reaction efficiency of 0.1 as default value (0.05-0.2 in Sander et al., 2011) and which is independent of temperature and acid composition. The reaction rate is proportional to  $\gamma$  and increases with aerosol SAD. For heterogeneous

55



1 reactions involving ClONO<sub>2</sub>, kinetics are taken from the well-detailed uptake model of Shi et al. (2001)  
2 which uses the parameterization of H<sub>2</sub>SO<sub>4</sub>/H<sub>2</sub>O composition of Tabazadeh et al. (1997). These processes  
3 are strongly functions of the acid composition and temperature. Note that the  $\gamma$  reaction efficiency for  
4 ClONO<sub>2</sub> described in the JPL recommendation of Sander et al. (2011) is taken from Shi et al. (2001).  
5 The BrONO<sub>2</sub> reactivity on sulfuric acid particles is computed from the JPL parameterization which is  
6 based on the work of Hanson (2003) and shows a rather limited dependence on acid composition and  
7 temperature.

8 Initialized amounts of species are taken from a 2D model long-term simulation (Bekki and Pyle,  
9 1994). Initialization of stratospheric chlorine precursors is based on scenarios defined by the World  
10 Meteorological Organization (WMO, 2014). Total inorganic chlorine ( $Cl_y = HCl + ClONO_2 + HOCl +$   
11  $ClO + Cl_2O_2$ ) is calculated by the model, and approaches 3.3 ppbv in the upper stratosphere in 2009, in  
12 accordance with the WMO (2014). Note that as expected this value is reduced compared to the study  
13 (3.7 ppbv) by Berthet et al. (2005). Total stratospheric inorganic bromine takes into account the  
14 contributions from Halons, methyl bromide and very-short-lived bromine compounds to reach 19.5 pptv,  
15 matching the scenario given by WMO (2010) updated from Dorf et al. (2006a). The 2D model  
16 climatology (Bekki and Pyle, 1994) also provides the initialization of H<sub>2</sub>SO<sub>4</sub> mixing ratios for the  
17 background aerosols. Liquid particles are formed in equilibrium and are assumed to have a predefined  
18 number density. Mean particle radii and SADs of the liquid aerosols are calculated from the number  
19 density and the amount of H<sub>2</sub>SO<sub>4</sub> and H<sub>2</sub>O assuming a lognormal unimodal distribution with a fixed  
20 distribution width.

21  
22



## 1 **References:**

- 2 Aliwell, S., Van Roozendaal, M., Johnston, P., Richter, A., Wagner, T., Arlander, D., Burrows, J., Fish,  
3 D., Jones, R., Tornkvist, K., Lambert, J.-C., Pfeilsticker, K., and Pundt, I.: Analysis for BrO in zenith-  
4 sky spectra: An intercomparison exercise for analysis improvement, *J. Geophys. Res.*, 107,  
5 doi:10.1029/2001JD000329, 4199 pp., 2002.
- 6
- 7 Bekki S. and Pyle J. A.: A two-dimensional study of the volcanic eruption of Mount Pinatubo, *Geophys.*  
8 *Res. Lett.*, 99, D9, 18,861-18,869, 1994.
- 9 Berthet, G., Renard, J.-B., Brogniez, C., Robert, C., Chartier, M., and Pirre, M., Optical and physical  
10 properties of stratospheric aerosols from balloon measurements in the visible and near-infrared domain:  
11 1. Analysis of aerosol extinction spectra from the AMON and SALOMON instruments, *Appl. Opt.*,  
12 41(36), 7522-7539, 2002.
- 13 Berthet, G., Ricaud, P., Lefèvre, F., Le Flochmoën, E., Urban, J., Barret, B., Lautié, N., Dupuy, E., De  
14 La Noë, J., and Murtagh, D.: Nighttime chlorine monoxide observations by the Odin satellite and  
15 implications on the Cl<sub>2</sub>O<sub>2</sub>/ClO equilibrium, *Geophys. Res. Lett.*, doi:10.1029/2005GL022649, 32,  
16 L11812, 2005.
- 17 Berthet, G., Huret, N., Lefèvre, F., Moreau, G., Robert, C., Chartier, M., Catoire, V., Barret, B., Pisso,  
18 I., and Pomathiod, L.: On the ability of chemical transport models to simulate the vertical structure of  
19 the N<sub>2</sub>O, NO<sub>2</sub> and HNO<sub>3</sub> species in the mid-latitude stratosphere, *Atmos. Chem. Phys.*, 6, 1599-1609,  
20 2006.
- 21 Berthet, G., Renard, J.-B., Catoire, V., Chartier, M., Robert, C., Huret, N., Coquelet, F., Bourgeois, Q.,  
22 Rivière, E. D., Barret, B., Lefèvre, F., and Hauchecorne, A.: Remote sensing measurements in the polar  
23 vortex: comparison to in situ observations and implications for the simultaneous retrievals and analysis  
24 of the NO<sub>2</sub> and OClO species, *J. Geophys. Res.*, 112, D21310, doi:10.1029/2007JD008699, 2007.
- 25
- 26 Borrmann, S., Solomon, S., Dye, J. E., Baumgardner, D., Kelly, K. K., and Roland Chan K.,  
27 Heterogeneous reactions on stratospheric background aerosols, volcanic sulfuric acid droplets, and type  
28 I polar stratospheric clouds: Effects of temperature fluctuations and differences in particle phase, *J.*  
29 *Geophys. Res.*, 102(D3), 3639-3648, 1997.
- 30 Bourassa, A. E., Rieger, L. A., Lloyd, N. D., and Degenstein, D. A.: Odin-OSIRIS stratospheric aerosol  
31 data product and SAGE III intercomparison, *Atmos. Chem. Phys.*, 12, 605-614, 2012.
- 32 Bracher, A., Sinnhuber, M., Rozanov, A., and Burrows, J. P.: Using a photochemical model for the  
33 validation of NO<sub>2</sub> satellite measurements at different solar zenith angles, *Atmos. Chem. Phys.*, 5, 393-  
34 408, 2005.
- 35 Brasseur, G., and C., Granier: Mount Pinatubo aerosols, chlorofluorocarbons and ozone depletion,  
36 *Science*, 257, 1239-1242, 1992.
- 37 Brohede, S., McLinden, C. A., Berthet, G., Haley, C. S., Murtagh, D., and Sioris, C. E.: Stratospheric  
38 NO<sub>2</sub> Climatology from Odin/OSIRIS Limb Scattering Measurements, *Can. J. Phys.*, 85(11), 1253-1274,  
39 2007.
- 40 Brohede, S., McLinden, C. A., Urban, J., Haley, C. S., Jonsson, A. I., and Murtagh, D.: Odin  
41 stratospheric proxy NO<sub>y</sub> measurements and climatology, *Atmos. Chem. Phys.*, 8, 5731-5754, 2008.



- 1 Brown, S. S., R. K. Talukdar, and A. R. Ravishankara, Rate constants for the reaction  $\text{OH} + \text{NO}_2 + \text{M}$   
2  $\rightarrow \text{HNO}_3 + \text{M}$  under atmospheric conditions, *Chem. Phys. Lett.*, 299, 277–284, 1999.  
3  
4 Brühl, C., Crutzen, P.J., and Grooss, J.-U.: High-latitude, summertime  $\text{NO}_x$  activation and seasonal  
5 ozone decline in the lower stratosphere: Model calculations based on observations by HALOE on  
6 UARS, *J. Geophys. Res.*, 103, D3, 3597-3597, 1998.
- 7 Bucholtz, A.: Rayleigh-scattering calculations for the terrestrial atmosphere, *Appl. Opt.*, 34, 1227–1230,  
8 1995.  
9  
10 Butz, A., Bösch, H., Camy-Peyret, C., Chipperfield, M., Dorf, M., Dufour, G., Grunow, K., Jeseck, P.,  
11 Kühl, S., Payan, S., Pepin, I., Pukite, J., Rozanov, A., von Savigny, C., Sioris, C., Wagner, T., Weidner,  
12 F., and Pfeilsticker, K.: Inter-comparison of stratospheric  $\text{O}_3$  and  $\text{NO}_2$  abundances retrieved from balloon  
13 borne direct sun observations and Envisat/SCIAMACHY limb measurements, *Atmos. Chem. Phys.*, 6,  
14 1293–1314, 2006.  
15  
16 Carn, S.A., Clarisse, L. and Prata, A. J.: Multi-decadal satellite measurements of global volcanic  
17 degassing, *J. Volcanol. Geotherm. Res.*, 311, 99–134, 2016.  
18  
19 Carslaw, K., Luo, B., and Peter, T.: An analytic expression for the composition of aqueous  $\text{HNO}_3$ - $\text{H}_2\text{SO}_4$   
20 stratospheric aerosols including gas phase removal of  $\text{HNO}_3$ , *Geophys. Res. Lett.*, 16, 1877-1880, 1995.  
21  
22 Chipperfield, M. P.: Multiannual simulations with a three-dimensional chemical transport model, *J.*  
23 *Geophys. Res.*, 104(D1), 1781-1805, 1999.
- 24 Clarisse, L., Hurtmans, D., Clerbaux, C., Hadji-Lazaro, J., Ngadi, Y., and Coheur, P.-F.: Retrieval of  
25 sulphur dioxide from the infrared atmospheric sounding interferometer (IASI), *Atmos. Meas. Tech.*, 5,  
26 581–594, doi:10.5194/amt-5-581-2012, 2012.  
27  
28 Coffey, M. T., and Mankin, W. G.: Observations of the loss of stratospheric  $\text{NO}_2$  following volcanic  
29 eruptions, 20(24), 2873-2876, *Geophys. Res. Lett.*, 1993.  
30  
31 Cox, R. A., MacKenzie, A. R., Müller, R. H., Peter, T., and Crutzen, P. J.: Activation of stratospheric  
32 chlorine by reactions in liquid sulphuric acid, *Geophys. Res. Lett.*, 21(13), 1439-1442, 1994.
- 33 Danilin, M. J., Rodriguez, J. M., Hu, W., Ko, M.K.W., Weisenstein, D.K., Kumer, J.B., Mergenthaler,  
34 J.L., Russell III, J.M., Koike, M., Yue, G.K., Jones, N.B., and Johnston, P.V.: Nitrogen species in the  
35 post-Pinatubo stratosphere: Model analysis utilizing UARS measurements, *J. Geophys. Res.*, 104(D7),  
36 8247-8262, 1999.  
37  
38 Deshler, T., Hervig, M. E., Hofmann, D. J., Rosen, J. M., and Liley, J. B.: Thirty years of in situ  
39 stratospheric aerosol size distribution measurements from Laramie, Wyoming ( $41^\circ\text{N}$ ), using balloon-  
40 borne instruments, *J. Geophys. Res.*, 108, 4167, doi:10.1029/2002JD002514, 2003.  
41  
42 Dorf, M., Butler, J. H., Butz, A., Camy-Peyret, C., Chipperfield, M. P., Kritten, L., Montzka, S. A.,  
43 Simmes, B., Weidner, F., and Pfeilsticker, K.: Long-term observations of stratospheric bromine reveal  
44 slow down in growth, *Geophys. Res. Lett.*, 33, L24803, doi:10.1029/2006GL027714, 2006a.  
45  
46 Dorf, M., Bösch, H., Butz, A., Camy-Peyret, C., Chipperfield, M. P., Engel, A., Goutail, F., Grunow,  
47 K., Hendrick, F., Hrechanyy, S., Naujokat, B., Pommereau, J.-P., Van Roozendaal, M., Sioris, C., Stroth,  
48 F., Weidner, F., and Pfeilsticker, K.: Balloonborne stratospheric  $\text{BrO}$  measurements: comparison with  
49 Envisat/SCIAMACHY  $\text{BrO}$  limb profiles, *Atmos. Chem. Phys.*, 6, 2483–2501, 2006b.  
50



- 1 Dufour, G., Payan, S., Lefèvre, F., Eremenko, M., Butz, A., Jeseck, P., Té, Y., Pfeilsticker, K., and  
2 Camy-Perret, C.: 4-D comparison method to study the NO<sub>y</sub> partitioning in summer polar stratosphere –  
3 Influence of aerosol burden, Atmos. Chem. Phys., 5, 919–926, 2005.  
4
- 5 Erle, F., Grendel, A., Perner, D., Platt, U., and Pfeilsticker, K.: Evidence of heterogeneous chemistry on  
6 cold stratospheric sulphate aerosols, Geophys. Res. Lett., Vol. 25, No. 23, 4329-4332, 1998.
- 7 Fahey, D. W., Kawa, S. R., Woodbridge, E. L., et al.: In situ measurements constraining the role of  
8 sulphate aerosols in mid-latitude ozone depletion, Vol. 363, 509-514, Nature, 1993.
- 9 Fahey, D. W., and A. R., Ravishankara: Summer in the stratosphere, Science, 285, n°5425, 208-210,  
10 1999.
- 11 Ferlemann, F., Camy-Peyret, C., Fitzenberger, R., Harder, H., Hawat, T., Osterkamp, H., Schneider, M.,  
12 Perner, D., Platt, U., Vradelis, P., and Pfeilsticker, K.: Stratospheric BrO profiles measured at different  
13 latitudes and seasons: Instrument description, spectral analysis and profile retrieval, Geophys. Res. Lett.,  
14 25, 3847–3850, 1998.  
15
- 16 Ferlemann, F., Bauer, N., Fitzenberger, R., Harder, H., Osterkamp, H., Perner, D., Platt, U., Schneider,  
17 M., Vradelis, P., and Pfeilsticker, K.: Differential Optical Absorption Spectroscopy Instrument for  
18 stratospheric balloon-borne trace gas studies, Applied Optics, 39, 2377 - 2386, 2000.  
19
- 20 Fischer, H. et al.: MIPAS: an instrument for atmospheric and climate research, Atmos. Chem. Phys., 8,  
21 2151-2188, 2008.
- 22 Gao, R. S., Fahey, D. W., et al.: A comparison of observations and model simulations of NO<sub>x</sub>/NO<sub>y</sub> in  
23 the lower stratosphere, Geophys. Res. Lett., 26, 1153– 1156, 1999.  
24
- 25 Granier, C., and Brasseur, G.: Impact of heterogeneous chemistry on model predictions of ozone  
26 changes, J. Geophys. Res., 97(D16), 18,015-18,033, 1992.  
27
- 28 Grossel, A., Huret, N., Catoire, V., Berthet, G., Renard, J.-B., Robert, C., and Gaubicher, B.: In situ  
29 balloon-borne measurements of HNO<sub>3</sub> and HCl stratospheric vertical profiles influenced by PSC  
30 formation during 2005-2006 Arctic winter, J. Geophys. Res., 115, D21303, doi:  
31 10.1029/2009JD012947, 2010.  
32
- 33 Hanson, D. R., Ravishankara, A. R., and Solomon, S.: Heterogeneous reactions in sulfuric acid aerosols:  
34 A framework for model calculations, J. Geophys. Res., 99(D2), 3615-3629, 1994.
- 35 Hanson, D. R., and Ravishankara, A. R., Heterogeneous chemistry of bromine species in sulfuric acid  
36 under stratospheric conditions, Geophys. Res. Lett., 22(4), 385-388, 1995.
- 37 Hanson, D. R., Ravishankara, A. R., and Lovejoy, E. R., Reaction of BrONO<sub>2</sub> with H<sub>2</sub>O on submicron  
38 sulfuric acid aerosol and the implications for the lower stratosphere, J. Geophys. Res., 101(D4), 9063-  
39 9069, 1996.
- 40 Hanson, D. R., Reactivity of BrONO<sub>2</sub> and HOBr on sulfuric acid solutions at low temperatures, J.  
41 Geophys. Res., 108(D8), 4239, doi:10.1029/2002JD002519, 2003.
- 42 Hanisco, T. F., Lanzendorf, E. J., Wennberg, P. O., Perkins, K. K., Stimpfle, R. M., Voss, P. B.,  
43 Anderson, J. G., Cohen, R. C., Fahey, D. W., Gao, R. S., Hints, E. J., Salawitch, R. J., Margitan, J. J.,  
44 McElroy, C. T., and Midwinter, C.: Sources, Sinks, and the Distribution of OH in the Lower  
45 Stratosphere, J. Phys. Chem. A, 2001, 105 (9), pp 1543–1553, 2001.





- 1 Harder, J.W., Brault, J.W., Johnston, P.V., and Mount, G.H.: Temperature dependent NO<sub>2</sub> cross sections  
2 at high spectral resolution, *J. Geophys. Res.*, 102, 3861-3879, 1997.
- 3 Harder, H., Camy-Peyret, C., Ferlemann, F., Fitzenberger, R., Hawat, T., Osterkamp, H., Perner, D.,  
4 Platt, U., Schneider, M., Vradelis, P., and Pfeilsticker, K.: Stratospheric BrO Profiles Measured at  
5 Different Latitudes and Seasons: Atmospheric Observations, *Geophys. Res. Lett.*, 25, 3843-3846, 1998.
- 6 Harder, H., Bösch, H., Camy-Peyret, C., Chipperfield, M., Fitzenberger, R., Payan, S., Perner, D., Platt,  
7 U., Sinnhuber, B., and Pfeilsticker, K.: Comparison of measured and modeled stratospheric BrO:  
8 Implications for the total amount of stratospheric bromine, *Geophys. Res. Lett.*, 27, 3695 - 3698, 2000.  
9
- 10 Harder, J. W., Brault, J. W., Johnston, P. V., and Mount, G. H.: Temperature dependent NO<sub>2</sub> cross  
11 sections at high spectral resolution, *J. Geophys. Res.*, 102, 3861–3879, 1997. Haywood, J. M., Jones, A.,  
12 Clarisse, L., Bourassa, A., Barnes, J., Telford, P., Bellouin, N., Boucher, O., Agnew, P., Clerbaux, C.,  
13 Coheur, P., Degenstein, D., and Braesicke, P.: Observations of the eruption of the Sarychev volcano and  
14 simulations using the HadGEM2 climate model, *J. Geophys. Res.*, 115, D21212,  
15 doi:10.1029/2010JD014447, 2010.  
16
- 17 Hofmann, D. J., and Solomon, S., Ozone destruction through heterogeneous chemistry following the  
18 eruption of El Chichon, *J. Geophys. Res.*, 94(D4), 5029-5041, 1989.
- 19 Hofmann, D. J., Oltmans, S. J., Komhyr, W. D., Harris, J. M., Lathrop, J. A., Langford, A. O., Deshler,  
20 T., Johnson, B. J., Torres, A., and W. Matthews, A.: Ozone loss in the lower stratosphere over the United  
21 States in 1992-1993: Evidence for heterogeneous chemistry on the Pinatubo aerosol, *Geophys. Res.*  
22 *Lett.*, 21(1), 65-68, 1994.  
23
- 24 Hormann, C., H. Sihler, N. Bobrowski, S. Beirle, M. Penning de Vries, U. Platt, and T. Wagner,  
25 Systematic investigation of bromine monoxide in volcanic plumes from space by using the GOME-2  
26 instrument, *Atmos. Chem. Phys.*, 13, 4749-4781, 2013.
- 27 Jégou, F., Berthet, G., Brogniez, C., Renard, J.-B., François, P., Haywood, J.M., Jones, A., Bourgeois,  
28 Q., Lurton, T., Auriol, F., Godin-Beekmann, S., Guimbaud, C., Krysztofiak, G., Gaubicher, B., Chartier,  
29 M., Clarisse, L., Clerbaux, C., Balois, J.-Y., Verwaerde, C., and Dauteron, D.: Stratospheric aerosols  
30 from the Sarychev volcano eruption in the 2009 Arctic summer, *Atmos. Chem. Phys.*, 13, 6533-6552,  
31 doi:10.5194/acp-13-6533-2013, 2013.
- 32 Johnston, P. V., McKenzie, R. L., Keys, J. G., and Matthews, W. A.: Observations of depleted  
33 stratospheric NO<sub>2</sub> following the Pinatubo volcanic eruption, *Geophys. Res. Lett.*, 19(2), 211-213, 1992.
- 34 Jucks, K. W., Johnson, D. G., Chance, K. V., Traub, W.A., and Salawitch, R. J.: Nitric acid in the middle  
35 stratosphere as a function of altitude and aerosol loading, *J. Geophys. Res.*, 104(D21), 26,715-26,723,  
36 1999.
- 37 Kinnison, D. E., Grant, K. E., Connell, P. S., Rotman, D. A., and Wuebbles, D. J.: The chemical and  
38 radiative effects of the Mount Pinatubo eruption, *J. Geophys. Res.*, 99, D12, 25,705-25,731, 1994.  
39
- 40 Koike, M., Kondo, Y., Matthews, W. A., Johnston, P. V., Yamazaki, K.: Decrease of stratospheric NO<sub>2</sub>  
41 at 44°N caused by Pinatubo volcanic aerosols, *Geophys. Res. Lett.*, 20(18), 1975-1978, 1993.  
42
- 43 Koike, M., Jones, N. B., Matthews, W. A., Johnston, P. V., McKenzie, R. L., Kinnison, D., and  
44 Rodriguez, J.: Impact of Pinatubo aerosols on the partitioning between NO<sub>2</sub> and HNO<sub>3</sub>, *Geophys. Res.*  
45 *Lett.*, 21(7), 597-600, 1994.



- 1 Kondo, Y., Kawa, S. R., Lary, D., Sugita, T., Douglass, A. R., Lutman, E., Koike, M., and Deshler, T.:  
2 Interpretation of nitric oxide profile observed in January 1992 over Kiruna, *J. Geophys. Res.*, 101(D7),  
3 12,555-12,566, 1996.
- 4  
5 Kondo, Y., Sugita, T., Salawitch, R. J., Koike, M., and Deshler, T.: Effect of Pinatubo aerosols on  
6 stratospheric NO, *J. Geophys. Res.*, 102(D1), 1205-1213, 1997.
- 7 Kondo, Y., Sugita, T., Koike, M., Kawa, S.R., Danilin, M. Y., Rodriguez, J. M., Spreng, S., Golinger,  
8 K., and Arnold, F.: Partitioning of reactive nitrogen in the midlatitude lower stratosphere, *J. Geophys.*  
9 *Res.*, 105(D1), 1417-1424, 2000.
- 10  
11 Kravitz, B., Robock, A., Bourassa, A., Deshler, T., Wu, D., Mattis, I., Finger, F., Hoffmann, A., Ritter,  
12 C., Bitar, L., Duck, T. J., and Barnes, J. E.: Simulation and observations of stratospheric aerosols from  
13 the 2009 Sarychev volcanic eruption, *J. Geophys. Res.*, 116, D18211, doi:10.1029/2010JD015501,  
14 2011.
- 15  
16 Krecl, P., Haley, C. S., Stegman, J., Brohede, S. M., and Berthet, G.: Retrieving the vertical distribution  
17 of stratospheric OClO from Odin/OSIRIS limb-scattered sunlight measurements, *Atmos. Chem. Phys.*,  
18 6, 1879-1894, 2006.
- 19 Kreycy, S. K., Camy-Peyret, C., Chipperfield, M.P., Dorf, M., Feng, W., Hossaini, R., Kritten, L.,  
20 Werner, B., and Pfeilsticker, K.: Atmospheric test of the  $J(\text{BrONO}_2)=k(\text{BrO}+\text{NO}_2)$  ratio: Implications  
21 for total stratospheric  $\text{Br}_y$  and bromine-mediated ozone loss, *Atmos. Chem. Phys.*, 13, 6263 - 6274,  
22 doi:10.5194/acp-13-6263-2013, 2013.
- 23  
24 Krysztofiak, G., Thiéblemont, R., Huret, N., Catoire, V., Té, Y., Jégou, F., Coheur, P. F., Clerbaux, C.,  
25 Payan, S., Drouin, M.A., Robert, C., Jeseck, P., Attié, J.-L., and Camy-Peyret, C.: Detection in the  
26 summer polar stratosphere of pollution plume from East Asia and North America by balloon-borne in  
27 situ CO measurements, *Atmos. Chem. Phys.*, doi:10.5194/acp-12-11889-2012, 12, 11889–11906, 2012.
- 28  
29 Krysztofiak, G., Té, Y., Catoire, V., Berthet, G., Toon, G. C., Jégou, F., Jeseck, P., and Robert, C.:  
30 Carbonyl sulfide variability with latitude in the atmosphere, *Atmos.-Ocean*, 53:1, 89-101, doi:  
31 10.1080/07055900.2013.876609, 2015.
- 32  
33 Küll, V., Riese, M., Tie, X., Wiemert, T., Eidmann, G., Offermann, D., and Brasseur, G. P.:  $\text{NO}_y$   
34 partitioning and aerosol influences in the stratosphere, *J. Geophys. Res.*, Vol. 107, D23, 8183,  
35 doi:10.1029/2001JD001246, 2002.
- 36  
37 Lary, D. J., Chipperfield, M. P., Toumi, R., and Lenton, T.: Heterogeneous atmospheric bromine  
38 chemistry, *J. Geophys. Res.*, 101(D1), 1489-1504, 1996.
- 39 Lefèvre, F., Brasseur, G. P., Folkins, I., Smith, A. K., and Simon, P.: Chemistry of the 1991-1992  
40 stratospheric winter : Three-dimensional model simulations, *J. Geophys. Res.*, 99, 9183-8195, 1994.
- 41  
42 Lefèvre, F., Figarol, F., Carslaw, K., and Peter, T.: The 1997 Arctic ozone depletion quantified from  
43 three-dimensional model simulations, *Geophys. Res. Lett.*, 25, 2425-2428, 1998.
- 44  
45 Legras, B., Pissot, I., Berthet, G., and Lefèvre, F.: Variability of the Lagrangian turbulent diffusivity in  
46 the lower stratosphere, *Atmos. Chem. Phys.*, 4, 1605–1622, 2005.
- 47  
48 Lindenmaier, R., Strong, K., Batchelor, R. L., Bernath, P. F., Chabrilat, S., Chipperfield, M. P., Daffer,  
49 W. H., Drummond, J. R., Feng, W., Jonsson, A. I., Kolonjari, F., Manney, G. L., McLinden, C., Ménard,  
50 R., and Walker, K. A.: A study of the Arctic  $\text{NO}_y$  budget above Eureka, Canada, *J. Geophys. Res.*, 116,  
51 D23302, doi:10.1029/2011JD016207, 2011.



- 1  
2 Livesey, N.J., et al.: Earth Observing System (EOS) Aura Microwave Limb Sounder (MLS) Version  
3 3.3 and 3.4 Level 2 Data Quality and Description Document. Tech. Rep. JPL D-33509. NASA Jet  
4 Propulsion Laboratory, California Institute of Technology, Pasadena, California (91109-8099, available  
5 at: <http://mhs.jpl.nasa.gov/data/datadocs.php>), 2011.
- 6  
7 McElroy, M. B., Salawitch, R. J., and Minschwaner, K.: The changing stratosphere, *Planet. Space. Sci.*,  
8 Vol. 40, No. 2/3, 373-401, 1992.
- 9 McGee, T. J., Newman, P., Gross, M., Singh, U., Godin, S., Lacoste, A.-M., and Mégie G., Correlation  
10 of ozone loss with the presence of volcanic aerosols, *Geophys. Res. Lett.*, 21(25), 2801-2804, 1994.
- 11 Mébarki, Y., Catoire, V., Huret, N., Berthet, G., Robert, C., and Poulet, G.: More evidence for very  
12 short-lived substance contribution to stratospheric chlorine inferred from HCl balloon-borne in situ  
13 measurements in the tropics, *Atmos. Chem. Phys.*, 10, 1–13, 2010.
- 14 Michelsen, H. A., Manney, G. L., Gunson, M. R., and Zander, R.: Correlations of stratospheric  
15 abundances of NO<sub>y</sub>, O<sub>3</sub>, N<sub>2</sub>O, and CH<sub>4</sub> derived from ATMOS measurements, *J. Geophys. Res.*, 103, 28  
16 347–28 359, 1998.
- 17  
18 Michelsen, H. A., Spivakovsky, C.M., and Wofsy, S. C.: Aerosol-mediated partitioning of stratospheric  
19 Cl<sub>y</sub> and NO<sub>y</sub> at temperatures above 200 K, *Geophys. Res. Lett.*, 26(3), 299-302, 1999.
- 20  
21 Mills, M. J., Langford, A. O., O’Leary, T. J., Arpag, K., Miller, H. L., Proffitt, M. H., Sander, R. W.,  
22 and Solomon, S.: On the relationship between stratospheric aerosols and nitrogen dioxide, *Geophys.*  
23 *Res. Lett.*, 20(12), 1187-1190, 1993.
- 24 Monge-Sanz, B. M., Chipperfield, M. P., Simmons, A. J., and Uppala, S. M.: Mean age of air and  
25 transport in a CTM: comparison of different ECMWF analyses, *Geophys. Res. Lett.*, 34, L04801,  
26 doi:10.1029/2006GL028515, 2007.
- 27  
28 Moreau, G., Robert, C., Catoire, V., Chartier, M., Camy-Peyret, C., Huret, N., Pirre, M., and Pomathiod,  
29 L.: A multi-species in situ balloon-borne instrument with six diode laser spectrometers, *Appl. Opt.*,  
30 44(28), 1–18, 2005
- 31  
32 Newchurch, M. J., Allen, M., Gunson, M. R., et al.: Stratospheric NO and NO<sub>2</sub> abundances from  
33 ATMOS solar-occultation measurements, *Geophys. Res. Lett.*, Vol. 23, No. 17, 1996.
- 34  
35 O’Neill, N. T., Perro, C., Saha, A., Lesins, G., Duck, T. J., Eloranta, E. W., Nott, G. J., Hoffman, A.,  
36 Karumudi, M. L., Ritter, C., Bourassa, A., Abboud, I., Carn, S. A., and Savastiouk, V.: Properties of  
37 Sarychev sulphate aerosols over the Arctic, *J. Geophys. Res.*, 117, D04203,  
38 doi:10.1029/2011JD016838, 2012.
- 39  
40 Osterman, G.B., Sen, B. Toon, G.C., Salawitch R.J., Margitan, J.J., and Blavier, J.-F.: Partitioning of  
41 NO<sub>y</sub> species in the summer Arctic stratosphere, *Geophys. Res. Lett.*, 26(8), 1157-1160, 1999.
- 42  
43 Ovarlez J., and Ovarlez, H.: Water vapour and aerosol measurements during SESAME, and the  
44 observation of low water vapour content layers, in *Polar Stratospheric Ozone, proceedings of the Third  
45 European Workshop, Air Pollution Rep. 56*, J. A. Pyle, N. R. P. Harris, and G. T. Amanatidis, eds.  
46 European Commission, Luxembourg, pp. 205–208, 1995.
- 47



- 1 Payan, S., Camy-Peyret, C., Jeseck, P., Hawat, T., Pirre, M., Renard, J.-B., Robert, C., Lefèvre, F.,  
2 Kanzawa, H., and Sasano, Y.: Diurnal and nocturnal distribution of stratospheric NO<sub>2</sub> from solar  
3 and stellar occultation measurements in the Arctic vortex: comparison with models and ILAS satellite  
4 measurements, *J. Geophys. Res.*, 104, 21 585–21 593, 1999.  
5  
6 Pitari, G., and Rizi, V.: An estimate of the chemical and radiative perturbation of stratospheric ozone  
7 following the eruption of Mt. Pinatubo, *J. Atmos. Sci.*, Vol. 50, No. 19, 1993.  
8  
9 Pitari, G., Aquila, V., Kravitz, B., Robock, A., Watanabe, S., Cionni, I., De Luca, N., Di Genova, G.,  
10 Mancini, E., and Tilmes, S.: Stratospheric response to sulfate geoengineering: Results from the  
11 Geoengineering Model Intercomparison Project (GeoMIP), *J. Geophys. Res.*, 119,  
12 doi:10.1029/2013JD020566, 2014.
- 13 Pommereau, J.-P., and Piquard, J.: Ozone and nitrogen dioxide vertical distributions by UV-visible solar  
14 occultation from balloons, *Geophys. Res. Lett.*, 21, 1227– 1230, 1994.  
15  
16 Portmann, R. W., Brown, S. S., Gierczak, T., Talukdar, R. K., Burkholder, J. B., and Ravishankara, A.  
17 R.: Role of nitrogen oxides in the stratosphere: a reevaluation based on laboratory studies, *Geophys.*  
18 *Res. Lett.*, 26(15), 2387-2390, 1999.  
19  
20 Prasad, S. S.: A modeling study of the stratospheric NO<sub>x</sub>/NO<sub>y</sub> and NO<sub>x</sub>/HNO<sub>3</sub> ratios : Single- versus  
21 dual-channeled mode of OH, NO<sub>2</sub> association, *J. Geophys. Res.*, 108, D15, 4474,  
22 doi:10.1029/2002JD002970, 2003.  
23  
24 Prather, M.: Catastrophic loss of stratospheric ozone in dense volcanic clouds, *J. Geophys. Res.*, 97, D9,  
25 10,187-10,191, 1992.
- 26 Randall, C. E., Lumpe, J. D., Bevilacqua, R. M., Hoppel, K. W., Shettle, E. P., Rusch, D. W., Gordley,  
27 L. L., Kreher, K., Pfeilsticker, K., Boesch, H., Toon, G., Goutail, F., and Pommereau, J.-P.: Validation  
28 of POAM III NO<sub>2</sub> measurements, *J. Geophys. Res.*, Vol. 107, D20, 4432, doi:10.1029/2001JD001520,  
29 2002.  
30  
31 Randel, W. J., Wu F., Russell III, J. M., Waters, J. W., and Froidevaux, L.: Ozone and temperature  
32 changes in the stratosphere following the eruption of Mount Pinatubo, *J. Geophys. Res.*, 100, D8,  
33 16,753-16,764, 1995.
- 34 Randeniya, L. K., Vohralik, P. F., Plumb, I. C., and Ryan, K. R., Heterogeneous BrONO<sub>2</sub> hydrolysis:  
35 effect on NO<sub>2</sub> columns and ozone at high latitudes in summer, *J. Geophys. Res.*, 102, D19, 23,543-  
36 23,557, 1997.
- 37 Renard, J.-B., Chartier, M., Robert, C., Chalumeau, G., Berthet, G., Pirre, M., Pommereau, J. P., and  
38 Goutail, F.: SALOMON: a new, light balloon borne UV-visible spectrometer for nighttime observations  
39 of stratospheric trace-gas species, *Appl. Opt.*, 39, 386–392, 2000.  
40  
41 Renard, J.-B., Taupin, F. G., Rivière, E. D., Pirre, M., Huret, N., Berthet, G., Robert, C., Chartier, M.,  
42 Pepe, F., and George, M.: Measurements and simulation of stratospheric NO<sub>3</sub> at Mid- and High-latitudes  
43 in the Northern Hemisphere, *J. Geophys. Res.*, 106, 32387-32399, 2001.  
44  
45 Renard, J.-B., Berthet, G., Robert, C., Chartier, M., Pirre, M., Brogniez, C., Herman, M., Verwaerde,  
46 C., Balois, J.-Y., Ovarlez, J., Ovarlez, H., Crespin, J., and Deshler, T.: Optical and physical properties  
47 of stratospheric aerosols from balloon measurements in the visible and near-infrared domain: II.  
48 Comparison of extinction, reflectance, polarization and counting measurements, *Appl. Opt.*, 41, 7540–  
49 7549, 2002.  
50



- 1 Renard, J.-B., Ovarlez, J., Berthet, G., Fussen, B., Vanhellemont, F., Brogniez, C., Hadamcik, E.,  
2 Chartier, M., and Ovarlez, H.: Optical and physical properties of stratospheric aerosols from balloon  
3 measurements in the visible and near-infrared domains. III. Presence of aerosols in the middle  
4 stratosphere, *Appl. Opt.*, 44, 4086–4095, doi:10.1364/AO.44.004086, 2005.  
5
- 6 Renard, J.-B., Brogniez, C., Berthet, G., Bourgeois, Q., Gaubicher, B., Chartier, M., Balois, J.-Y.,  
7 Verwaerde, C., Auriol, F., François, P., Daugeron, D., and Engrand, C.: Vertical distribution of the  
8 different types of aerosols in the stratosphere, Detection of solid particles and analysis of their spatial  
9 variability, *J. Geophys. Res.*, 113, D21303, doi:10.1029/2008JD010150, 2008.  
10
- 11 Renard, J.-B., Berthet, G., Salazar, S., Catoire, V., Tagger, T., Gaubicher, B., and Robert, C.: In situ  
12 detection of aerosol layers in the middle stratosphere, *Geophys. Res. Lett.*, 37, L20803,  
13 doi:10.1029/2010GL044307, 2010.  
14
- 15 Rinsland, C. P., Weisenstein, D. K., Ko, M. K. W., Scott, C. J., Chiou, L. S., Mahieu, E., Znader, R.,  
16 and Demoulin, P.: Post-Mount Pinatubo eruption ground-based infrared stratospheric column  
17 measurements of HNO<sub>3</sub>, NO, and NO<sub>2</sub> and their comparison with model calculations, *J. Geophys. Res.*,  
18 108, D15, doi:10.1029/2002JD002965, 2003.
- 19 Rivière, E. D., Pirre, M., Berthet, G., Renard, J.-B., and Lefèvre, F.: Investigating the OCIO and Br<sub>y</sub>  
20 chemistry from high-latitude nighttime measurements of OCIO and NO<sub>2</sub>, *J. Atmos. Chem.*, 48, 261-282,  
21 2004.
- 22 Robock, A.: Volcanic eruptions and climate, *Rev. Geophys.*, 38, 2, 191-219, 2000.
- 23 Rodgers, C.: Inverse methods for atmospheric sounding: theory and practice, xvi-238 p.:ill., World  
24 scientific publishing, 2000.
- 25 Rodriguez, J. M., Ko, M. K. W., and Sze N. D., Role of heterogeneous conversion of N<sub>2</sub>O<sub>5</sub> on sulphate  
26 aerosols in global ozone losses, *Nature*, 352, 134-137, 1991.
- 27 Rothman, L. S., Gordon, I. E., Babikov, Y., Barbe, A., Benner, D. C., Bernath, P. F., et al.: The  
28 HITRAN2012 molecular spectroscopic database, *J. Quant. Spectrosc. Radiat. Transfer*, 130, 4–50,  
29 doi:10.1016/j.jqsrt.2013.07.002, 2013.  
30
- 31 Salawitch, R. J., Wofsy, S. C., Wennberg, P. O., et al.: The distribution of hydrogen, nitrogen, and  
32 chlorine radicals in the lower stratosphere: Implications for changes in O<sub>3</sub> due to emission of NO<sub>y</sub> from  
33 supersonic aircraft, *Geophys. Res. Lett.*, 21(23), 2547-2550, 1994a.  
34
- 35 Salawitch, R. J., Wofsy, S. C., Wennberg, P. O., et al., The diurnal variation of hydrogen, nitrogen, and  
36 chlorine radicals: Implications for the heterogeneous production of HNO<sub>2</sub>, *Geophys. Res. Lett.*, 21(23),  
37 2551-2554, 1994b.  
38
- 39 Salawitch, R. J., Weisenstein, D. K., Kovalenko, L. J., Sioris, C. E., Wennberg, P. O., Chance, K., Ko,  
40 M. K. W., and McLinden, C. A.: Sensitivity of ozone to bromine in the lower stratosphere, *Geophys.*  
41 *Res. Lett.*, 32, L05811, doi:10.1029/2004GL021504, 2005.  
42
- 43 Sander, S. P., Abbatt, J. P. D., Friedl, R. R., Barker, J. R., Burkholder, J. B., Golden, D. M., Kolb, C.  
44 E., Kurylo, M. J., Moortgat, G. K., Wine, P. H., Huie, R. E., Orkin, V. L.: Chemical kinetics and  
45 photochemical data for use in atmospheric studies, Evaluation number 17, *JPL Publ.*, 10-6, 684 pp.,  
46 2011.  
47



- 1 Santee, M. L., Manney, G. L., Livesey, N. J., and Read, W. G.: Three-dimensional structure and  
2 evolution of stratospheric HNO<sub>3</sub> based on UARS Microwave Limb Sounder measurements, 109,  
3 D15306, doi:10.1029/2004JD004578, 2004.
- 4
- 5 Sen, B., Toon, G. C., Osterman, G. B., Blavier, J.-F., Margitan, J. J., Salawitch, R. J., and Yue, G. K.:  
6 J. Geophys. Res., 103, D3, 3571-3585, 1998.
- 7
- 8 Shi, Q., Jayne, J. T., Kolb, C. E., and Worsnop, D. R.: Kinetic model for reaction of ClONO<sub>2</sub> with H<sub>2</sub>O  
9 and HCl and HOCl with HCl in sulfuric acid solutions, J. Geophys. Res., 106, D20, 24,259-24,274,  
10 2001.
- 11 Solomon, S., Sanders, R. W., Jakoubek, R. O., Arpag, K. H., Stephens, S. L., Keys, J. G., and Garcia, R.  
12 R.: Visible and near-ultraviolet spectroscopy at McMurdo Station, Antarctica. 10. Reductions of  
13 stratospheric NO<sub>2</sub> due to Pinatubo aerosols, J. Geophys. Res., 99(D2), 3509-3516, 1994.
- 14 Solomon, S., Portmann, R. W., Garcia, R. R., Thomason, L. W., Poole, L. R., and McCormick, M. P.:  
15 The role of aerosol variations in anthropogenic ozone depletion at northern midlatitudes, J. Geophys.  
16 Res., 101(D3), 6713-6727, 1996.
- 17 Solomon, S., Stratospheric ozone depletion: a review of concepts and history, Rev. Geophys., 37, 3,  
18 275-316, 1999.
- 19 Steele, H. M., and R. P., Turco, Retrieval of aerosol size distributions from satellite extinction spectra  
20 using constrained linear inversion, J. Geophys. Res., 102(D14), 16,737-16,747, 1997.
- 21 Stowasser, M., Oelhaf, H., Ruhnke, R., Kleinert, A., Wetzel, G., Friedl-Vallon, F., Kouker, W., Lengel,  
22 A., Maucher, G., Nordmeyer, H., Reddmann, T., and Fischer, H.: The variation of shortlived NOy  
23 species around sunrise at mid-latitudes as measured by MIPAS-B and calculated by KASIMA, Geophys.  
24 Res. Lett., 30, 1432, doi:10.1029/2002GL016727, 2003.
- 25
- 26 Swartz, W. H., Yee, J.-H., Randall, C. E., Shetter, R. E., Browell, E. V., Burris, J. F., McGee, T. J., and  
27 Avery, M. A.: Comparison of high latitude line of sight ozone column density with derived ozone fields  
28 and the effects of horizontal inhomogeneity, Atmos. Chem. Phys., 6, 1843–1852, 2006.
- 29
- 30 Tabazadeh, A., Toon, O. B., Clegg, S. L., and Hamill, P.: A new parameterization of H<sub>2</sub>SO<sub>4</sub>/H<sub>2</sub>O aerosol  
31 composition: Atmospheric implications, Geophys. Res. Lett., 24, 1931-1934, 1997.
- 32
- 33 Telford, P., Braesicke, P., Morgenstern, O., and Pyle, J.: Reassessment of causes of ozone column  
34 variability following the eruption of Mount Pinatubo using a nudged CCM, Atmos. Chem. Phys., 9,  
35 4251–4260, 2009.
- 36
- 37 Tie, X., Brasseur, G. P., Briegleb, B., and Granier, C., Two-dimensional simulation of Pinatubo aerosol  
38 and its effect on stratospheric ozone, J. Geophys. Res., 99, D10, 20,545-20,562, 1994.
- 39 Tie, X., and Brasseur, G.: The response of stratospheric ozone to volcanic eruptions: Sensitivity to  
40 atmospheric chlorine loading, Geophys. Res. Lett., Vol. 22, No. 22, 3035-3038, 1995.
- 41
- 42 Tie, X., and Brasseur, G. P.: The importance of heterogeneous bromine chemistry in the lower  
43 stratosphere, Geophys. Res. Lett., Vol. 23, No. 18, 2505-2508, 1996.
- 44 Van de Hulst, H. C.: Light Scattering By Small Particles, JohnWiley & Sons, Inc., New York, 1957.
- 45
- 46 Vernier, J.-P., Thomason, L. W., Pommereau, J.-P., Bourassa, A., Pelon, J., Garnier, A., Hauchecorne,  
47 A., Blanot, L., Trepte, C., Degenstein, D., and Vargas, F.: Major influence of tropical volcanic eruptions



- 1 on the stratospheric aerosol layer during the last decade, *Geophys. Res. Lett.*, 38, L12807,  
2 doi:10.1029/2011GL047563, 2011.
- 3
- 4 Wahner, A., Ravishankara, A., Sander, S., and Friedl, R.: Absorption cross section of BrO between 312  
5 and 385 nm at 298 and 223 K, *Chem. Phys. Lett.*, 152, 507–512, 1988.
- 6
- 7 Webster, C. R., May, R. D., Allen, M., Jaeglé, L., and McCormick M. P.: Balloon profiles of  
8 stratospheric NO<sub>2</sub> and HNO<sub>3</sub> for testing the heterogeneous hydrolysis of N<sub>2</sub>O<sub>5</sub> on sulfate aerosols,  
9 *Geophys. Res. Lett.*, Vol. 21, No. 1, 53-56, 1994.
- 10 Webster, C. R., May, R. D., Michelsen, H. A., et al.: Evolution of HCl concentrations in the lower  
11 stratosphere from 1991 to 1996 following the eruption of Mt. Pinatubo, *Geophys. Res. Lett.*, 25(7), 995-  
12 998, 1998.
- 13
- 14 Webster, C. R., Michelsen, H. A., Gunson, M. R., Margitan, J. J., Russell III, J. M., Toon, G. C., and  
15 Traub, W. A., J.: Response of lower stratospheric HCl/Cl<sub>y</sub> to volcanic aerosols: Observations from  
16 aircraft, balloon, space shuttle, and satellite instruments, *Geophys. Res.*, 105, D9, 11,711-11,719, 2000.
- 17
- 18 Weisenstein, D. K., Ko, M. K. W., Rodriguez, J. M., and N.-D. Sze.: Impact of heterogeneous chemistry  
19 on model-calculated ozone change due to high speed civil transport aircraft, *Geophys. Res. Lett.*, Vol.  
20 18, No. 11, 1991-1994, 1991.
- 21 Wennberg, P. O., Cohen, R. C., Stimpfle, R. M., et al.: Removal of stratospheric O<sub>3</sub> by radicals: in situ  
22 measurements of OH, HO<sub>2</sub>, NO, NO<sub>2</sub>, ClO and BrO, *Science*, 266, 398-404, 1994.
- 23 Wennberg, P. O., Hanisco, T. F., Cohen, R. C., Stimpfle R. M., Lapson, L. B. and Anderson, J. G.: In  
24 situ measurements of OH and HO<sub>2</sub> in the upper troposphere and stratosphere, *J. Atmos. Sci.*, Vol. 52,  
25 No. 19, 3413-3420, 1995.
- 26 Wetzel, G., Oelhaf, H., Ruhnke, R., Friedl-Vallon, F., Kleinert, A., Kouker, W., Maucher, G.,  
27 Reddman, T., Seefeldner, M., Stowasser, M., Trieschmann, O., Von Clarmann, T., and Fischer, H.:  
28 NO<sub>y</sub> partitioning and budget and its correlation with N<sub>2</sub>O in the Arctic vortex and in summer  
29 midlatitudes in 1997, *J. Geophys. Res.*, 107(D16), doi:10.1029/2001JD000916, 2002.
- 30
- 31 Willeke, K. and Liu, B. Y. H.: Single particle optical counter: principle and application, in *Fine Particles,*  
32 *Aerosol Generation, Measurement, Sampling and Analysis*, B. Y. H. Liu, ed. Academic, Orlando, Fla.,  
33 698–729, 1976.
- 34
- 35 Wiscombe, W. J.: Improved Mie scattering algorithms, *Appl. Opt.*, 19, 1505– 1509, 1980.
- 36
- 37 World Meteorological Organization (WMO): Scientific Assessment of Ozone Depletion, Report No 52,  
38 Geneva, 2010.
- 39
- 40 World Meteorological Organization (WMO): Scientific Assessment of Ozone Depletion, Report No 55,  
41 Geneva, 2014.
- 42



1 **Table 1:** Averaged percentage differences between model calculations and balloon-borne observations  
 2 (with respect to the measured profile) below 19 km. The model outputs from the one-dimensional  
 3 version are provided for the SPIRALE flights (see text).

4

Balloon flight	Observed species	Ref-sim	Bal-sim	Sat-sim	sim	Bal-sim
		3D version (no volcanic aerosols)	3D version (aerosols from balloon data)	3D version (aerosols from satellite data)	1D version (no volcanic aerosols)	1D version (aerosols from balloon data)
SPIRALE 7 August 2009 around 02H15 UT	NO <sub>2</sub>	+57%	+3±20%	+7%	+54%	+20%
	HNO <sub>3</sub>	-3%	+8±4%	+8%	-5%	+3%
	NO <sub>2</sub> /HNO <sub>3</sub>	+62%	-3±19%	-1%	+60%	+16%
SPIRALE 24 August 2009 around 21H15 UT	NO <sub>2</sub>	+56%	-16±20%	-5%	+42%	-7%
	HNO <sub>3</sub>	-4%	+8±3%	+6%	-4%	+6%
	NO <sub>2</sub> /HNO <sub>3</sub>	+63%	-22±20%	-10%	+48%	-12%
SALOMON 25 August 2009 around 19H30 UT	NO <sub>2</sub>	+51%	-16±17%	-5%	-	-
	BrO	-66%	-34±12%	-47%	-	-
DOAS 7 September 2009 around 15H45 UT	NO <sub>2</sub>	+75%	-12±16%	-7%	-	-
	BrO	-20%	12±6%	+9%	-	-

5

6

7

8

9

10

11

12

13

14

15

16

17




 1  
 2  
 3  
 4  
 5  
 6  
 7

**Table 2:** Averaged percentage differences between the aerosol-constrained and the reference simulations (with respect to the reference) at the dates of the various balloon flights. Differences are provided for 3D and 1D REPROBUS simulations. Calculations are done below 19 km where observations are available, i.e. for the same levels as in **Table 1**.

Date	Species	Bal-sim (3D)	Sat-sim (3D)	Ref-sim (1D)	Bal-sim (1D)	Bal-sim (1D)
		- Ref-sim (3D)	- Ref-sim (3D)	- Ref-sim (3D)	- Ref-sim (3D)	- Ref-sim (1D)
7 August 2009 around 02H15 UT	NO <sub>2</sub>	-34±13%	-31%	-3%	-24%	-22%
	HNO <sub>3</sub>	+10±4%	+9%	+7%	+15%	+8%
	NO <sub>2</sub> /HNO <sub>3</sub>	-40±13%	-36%	-9%	-34%	-27%
24 August 2009 around 21H15 UT	NO <sub>2</sub>	-46±12%	-39%	-9%	-41%	-34%
	HNO <sub>3</sub>	+13±3%	+11%	+2%	+13%	+11%
	NO <sub>2</sub> /HNO <sub>3</sub>	-52±12%	-44%	-10%	-47%	-41%
25 August 2009 around 19H30 UT	NO <sub>2</sub>	-47±10%	-40%	-	-	-
	BrO	181±74%	128%	-	-	-
7 September 2009 around 15H45 UT	NO <sub>2</sub>	-50±8%	-47%	-	-	-
	BrO	38±8%	34%	-	-	-

 8  
 9



1

2

3 **Table 3:** Simulated changes on various stratospheric key species due to the Sarychev volcanic aerosols  
 4 over the August-September 2009 period at 16.5 km. Calculations are done from the Sat-sim  
 5 simulation. Effects for daytime and nighttime conditions are provided depending on statistically  
 6 significant amounts in the diurnal cycle of a given compound. The contribution of BrONO<sub>2</sub> hydrolysis  
 7 to changes on the various species is also shown (see text).

8

9

Species	All chemistry				BrONO <sub>2</sub> hydrolysis effect	
	12H UT		00H UT		12H UT	00H UT
NO <sub>x</sub>	-0.23 ppbv	-44%	-0.19 ppbv	-48%	1.8%	1.1%
NO <sub>2</sub>	-0.12 ppbv	-43%	-0.19 ppbv	-48%	1.8%	1.1%
NO	-0.11 ppbv	-45%	---	---	2.0%	---
HNO <sub>3</sub>	+0.31 ppbv	+11%	+0.31 ppbv	+11%	-2.3%	-0.9%
N <sub>2</sub> O <sub>5</sub>	-0.08 ppbv	-80%	-0.12 ppbv	-66%	-3.6%	-3.1%
ClONO <sub>2</sub>	+0.02 ppbv	+16%	+0.02 ppbv	+22%	66.2%	60.6%
HCl	-0.02 ppbv	-3%	-0.02 ppbv	-3%	58.8%	58.9%
ClO <sub>x</sub>	+5.77 pptv	+106%	---	---	39.3%	---
ClO	+5.77 pptv	+106%	---	---	39.3%	---
HOCl	+2.17 pptv	+217%	+1.16 pptv	+346%	47.4%	50.1%
BrONO <sub>2</sub>	-1.37 pptv	-33%	-4.15 pptv	-70%	18.3%	98%
BrO	+0.94 pptv	+22%	---	---	16.2%	---
HOBr	---	---	+3.89 pptv	+141%	---	98.8%
HO <sub>x</sub>	+1.41 pptv	+51%	---	---	24.1%	---
OH	+0.05 pptv	+16%	---	---	44.1%	---
HO <sub>2</sub>	+1.36 pptv	+56%	---	---	23.1%	---
O <sub>3</sub>	-13.1 ppbv	-1.1%	-12.6 ppbv	-1.1%	22.5%	26.3%

10

11

12

13

14

15

16

17

18

19

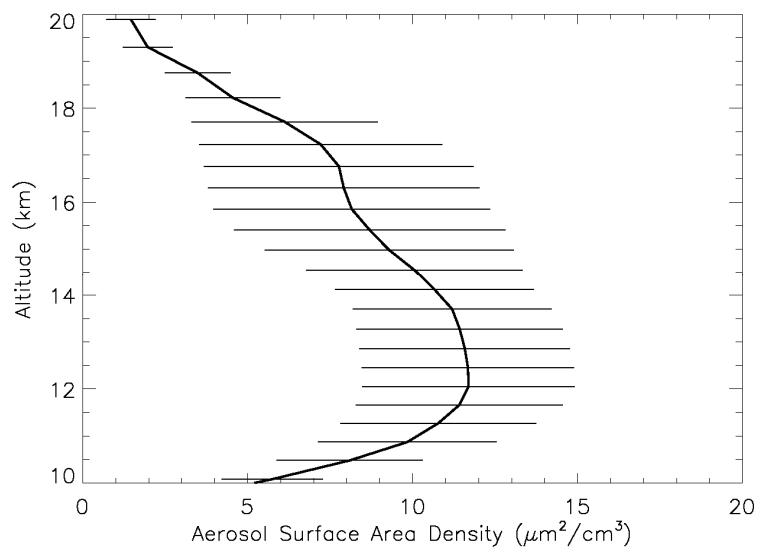
20

21

22



1  
2  
3



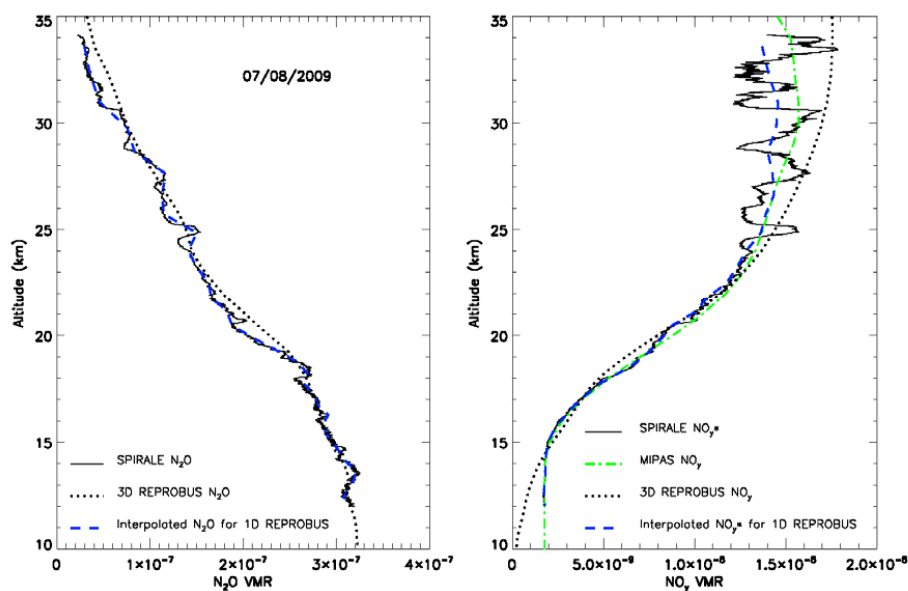
4

5 **Figure 1:** Range of aerosol SAD values derived from several balloon-borne observations in the lower  
6 stratosphere in summer 2009. Based on Table 1 in the work of Jégou et al. (2013) this average profile  
7 excludes data supposed to be spoiled by balloon outgassing as revealed from simultaneous in situ  
8 water vapour observations.

9  
10  
11  
12  
13  
14  
15  
16  
17  
18  
19



1  
2  
3



4

5 **Figure 2:** In situ vertical profiles recorded by the SPIRALE instrument used to constrain 1D  
6 simulations of the REPROBUS model. Left: profile of N<sub>2</sub>O recorded on 7 August 2009 (black line)  
7 compared to the results from the 3D version of REPROBUS (dotted line). Right: profile of NO<sub>y</sub>  
8 inferred from N<sub>2</sub>O observations converted using the N<sub>2</sub>O-NO<sub>y</sub> correlation curve presented in **Figure 3**  
9 (referred to as NO<sub>y</sub>\*). Also shown are the NO<sub>y</sub> profiles from the 3D version of REPROBUS (dotted  
10 line) and the MIPAS averaged data (green line). The 1D version of REPROBUS is computed with  
11 the profiles interpolated to the model resolution (blue lines).

12

13

14

15

16

17

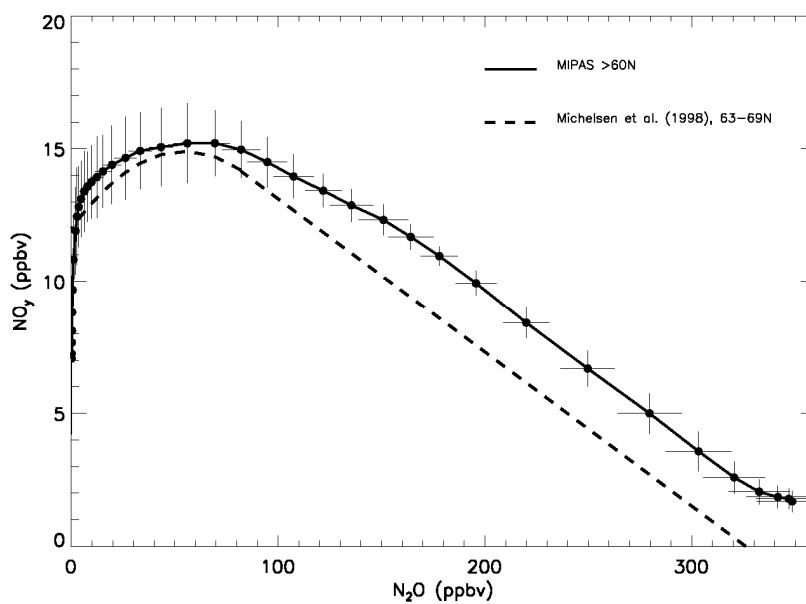
18

19

20



1  
2  
3



4

5 **Figure 3:** N<sub>2</sub>O-NO<sub>y</sub> correlation curve inferred from IMK/IAA V5R\_220 MIPAS-Envisat data at high  
6 latitudes (> 60°N) in July-August 2009 (full line). Error bars reflect the spread of the data. The former  
7 Michelsen et al. (1998) correlation is also shown for comparison (dashed line).

8

9

10

11

12

13

14

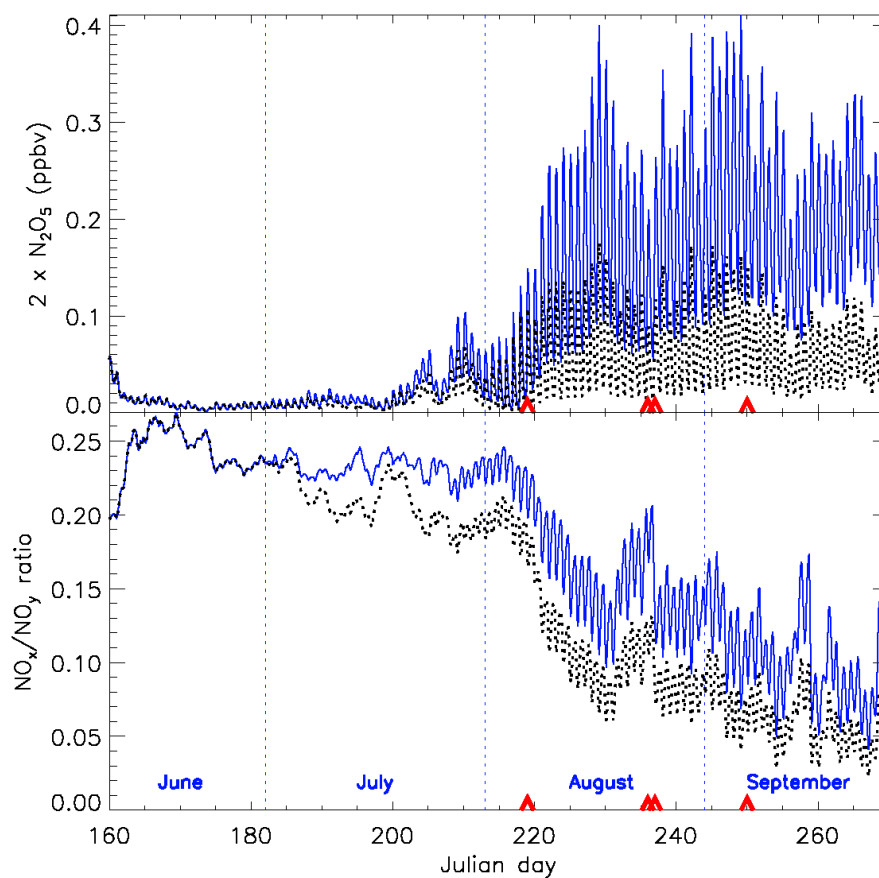
15

16

17



1  
2  
3



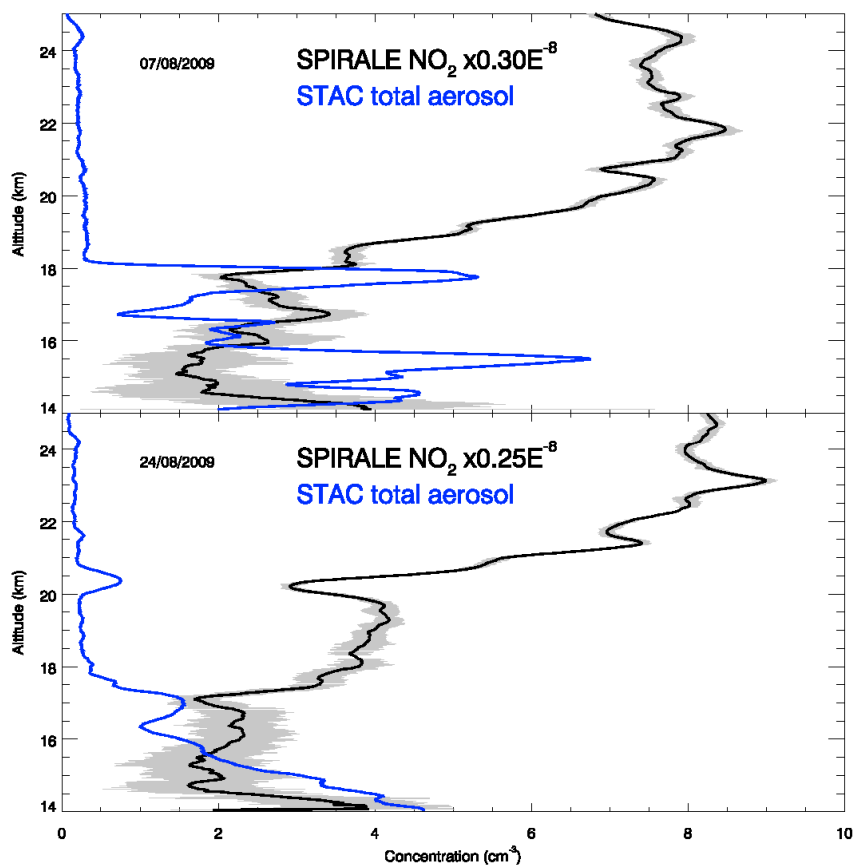
4  
5

6 **Figure 4:** Seasonal variation of  $\text{N}_2\text{O}_5$  (a) and of the  $\text{NO}_x/\text{NO}_y$  ratio (b) simulated by the REPROBUS  
7 CTM above Kiruna in Northern Sweden ( $67.5^\circ\text{N}$ ,  $21.0^\circ\text{E}$ ) around 17.5 km. The simulation driven by  
8 non-volcanic aerosol contents (Ref-sim) is shown in blue. The black dotted line is the REPROBUS  
9 simulation driven by volcanic aerosol levels from STAC balloon-borne observations (Bal-sim). Red  
10 triangles represent the dates of the balloon flights.  $\text{N}_2\text{O}_5$  recovery is onset at the beginning of August  
11 (day 213 is August 1, 2009) i.e. when SZA become  $>90^\circ$ .

12  
13  
14



1  
2  
3



4

5 **Figure 5:** Vertical profiles of NO<sub>2</sub> observed by the SPIRALE balloon-borne instrument (black line) on  
6 7 and 24 August 2009 compared to the total aerosol concentration profiles simultaneously recorded by  
7 the STAC aerosol counter (blue line) above Kiruna during balloon ascent. SPIRALE data have been  
8 averaged over 250 m (corresponding to ~1 minute of measurements).

9

10

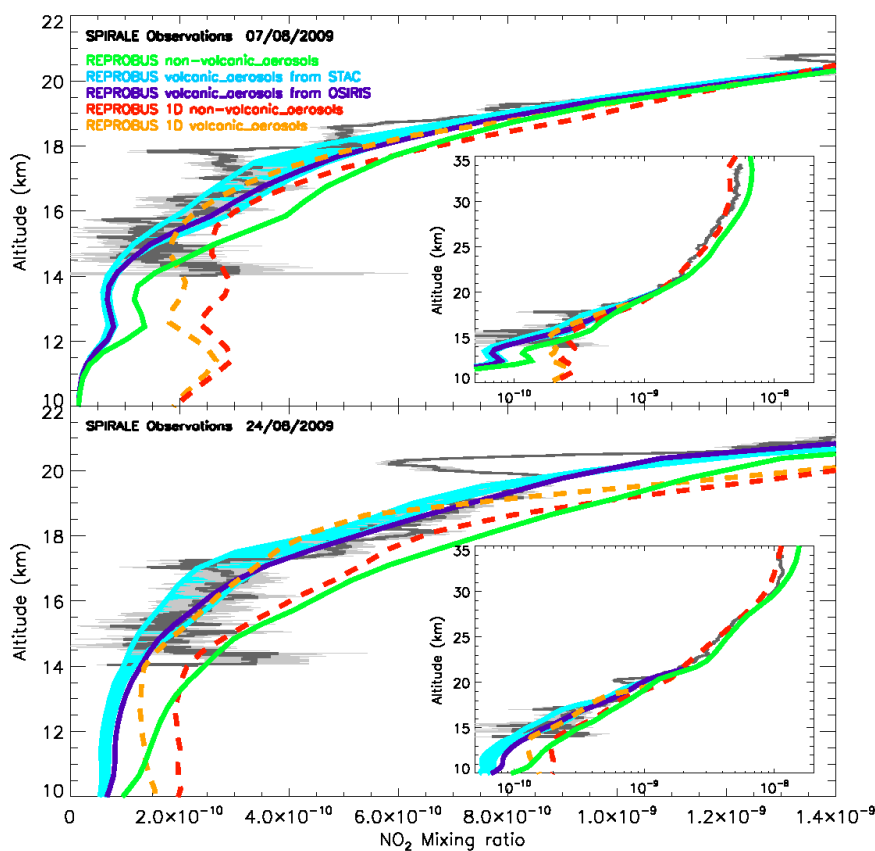
11

12

13



1  
2  
3



4  
5

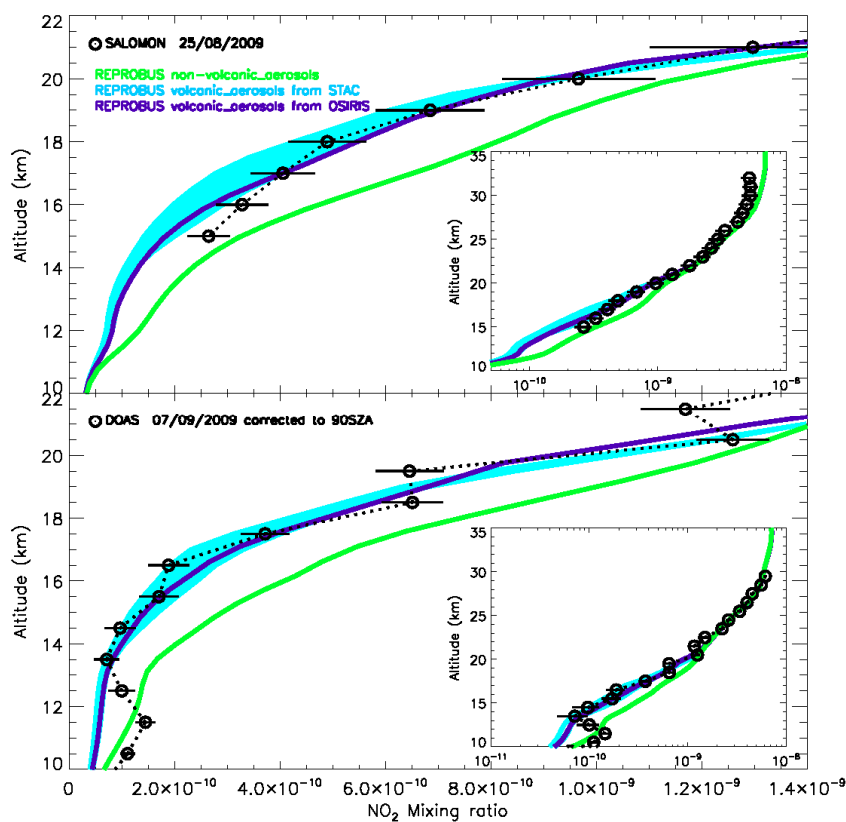
6 **Figure 6:** Vertical profile of  $\text{NO}_2$  observed by the SPIRALE balloon-borne instrument (black line)  
7 above Kiruna during balloon ascent between 02:00 and 02:30 UT for the 7 August 2009 flight (top)  
8 and between 21:00 and 21:30 UT for the 24 August 2009 flight (bottom). Model outputs (available  
9 every 15 minutes) are provided for the closest location of the instrument and interpolated to the time  
10 of observations. Three-dimensional simulations have been driven without volcanic aerosols (green),  
11 with volcanic aerosols from balloon-borne observations (blue shaded area) and with volcanic aerosols  
12 from satellite data (dark blue line). Results from a one-dimensional (1D) version of the REPROBUS  
13 model (dashed lines) computed using hybrid  $\text{NO}_y$  profiles ( $\text{NO}_y^*$ ) derived from the observed profiles  
14 of  $\text{N}_2\text{O}$  are also provided (see text), with in red the non-volcanic reference simulations and in orange  
15 the calculations driven with volcanic aerosols from the mean observed balloon-borne profile presented  
16 in **Figure 1**.

17





1  
2  
3



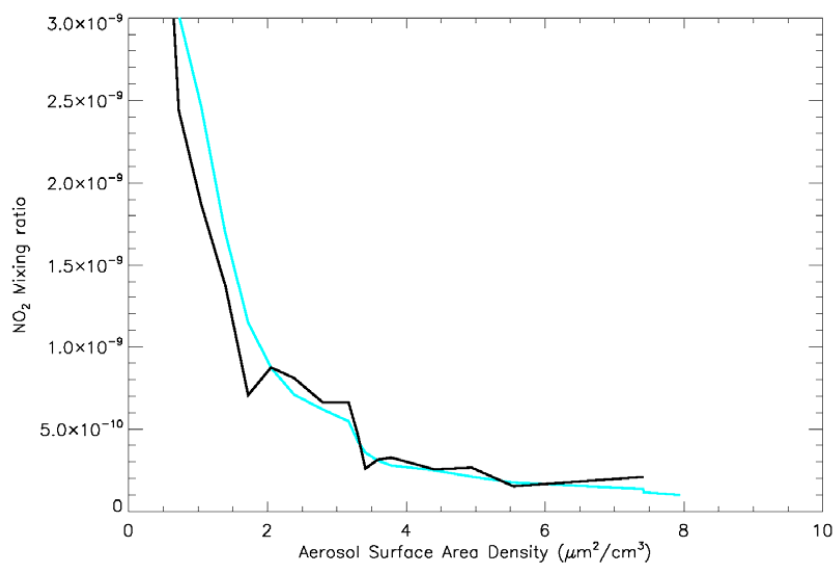
4

5 **Figure 7:** (top) Vertical profile of  $\text{NO}_2$  recorded by the SALOMON instrument (black lines) obtained  
6 during solar occultation between 18:50 and 19:30 UT on 25 August 2009 above Kiruna. Chemistry-  
7 transport model simulations computed with no volcanic aerosols (green line), with volcanic aerosols  
8 from balloon-borne observations (blue shaded area) and with volcanic aerosols from satellite data  
9 (dark blue line) are shown. The model output is provided for the closest location of the tangent points.  
10 (bottom) Vertical profile of  $\text{NO}_2$  recorded by the DOAS instrument (black lines) on 7 September 2009  
11 above Kiruna. The DOAS profile has been recorded during the balloon ascent and has been converted  
12 to  $90^\circ\text{SZA}$  ( $\sim 17:30$  UT) as well as the simulated profile.

13  
14  
15  
16



1  
2  
3



4

5 **Figure 8:** NO<sub>2</sub> mixing ratio as a function of aerosol SAD as simultaneously observed in the lower  
6 stratosphere by the SPIRALE and STAC instruments on 24 August 2009 (black curve). The result  
7 from the REPROBUS Bal-sim simulation is also plotted (blue curve).

8

9

10

11

12

13

14

15

16

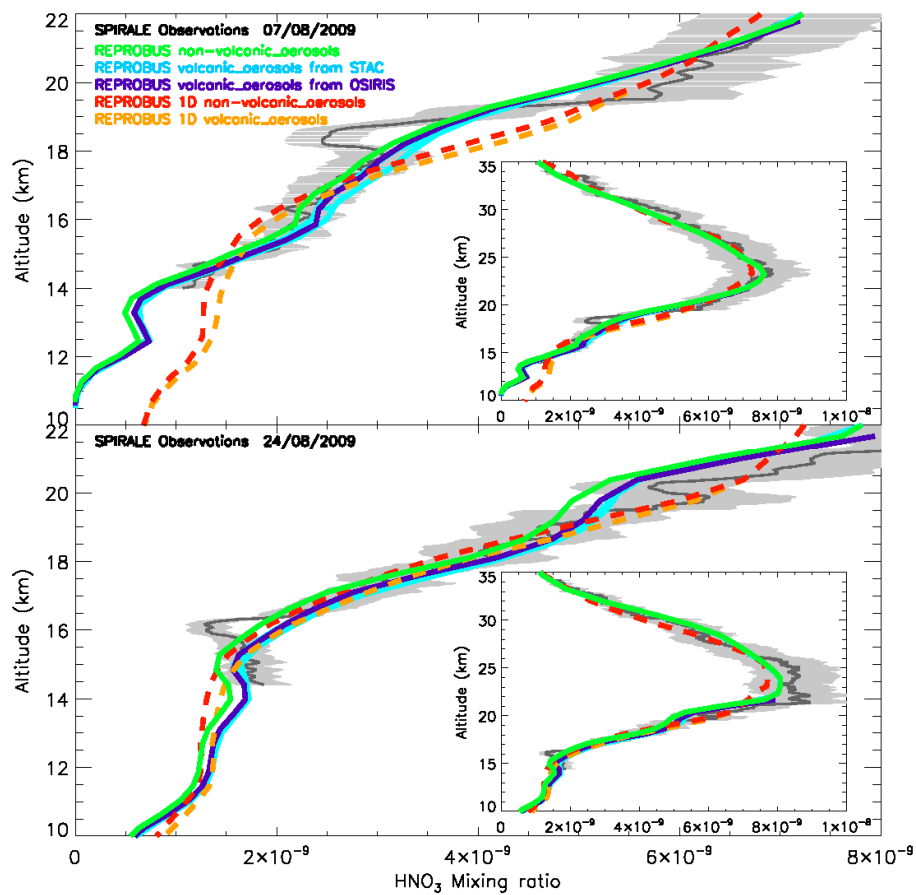
17

18

19



1  
2  
3

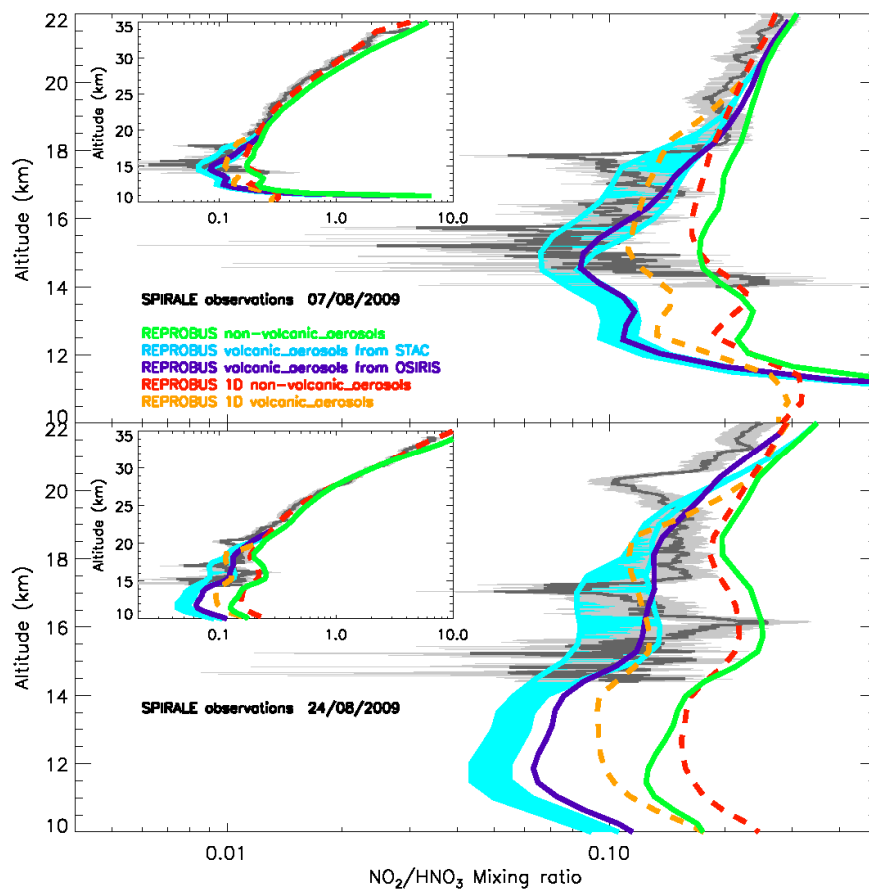


4  
5  
6  
7  
8  
9  
10  
11

Figure 9: same as Figure 6 but for HNO<sub>3</sub>.



1  
2  
3

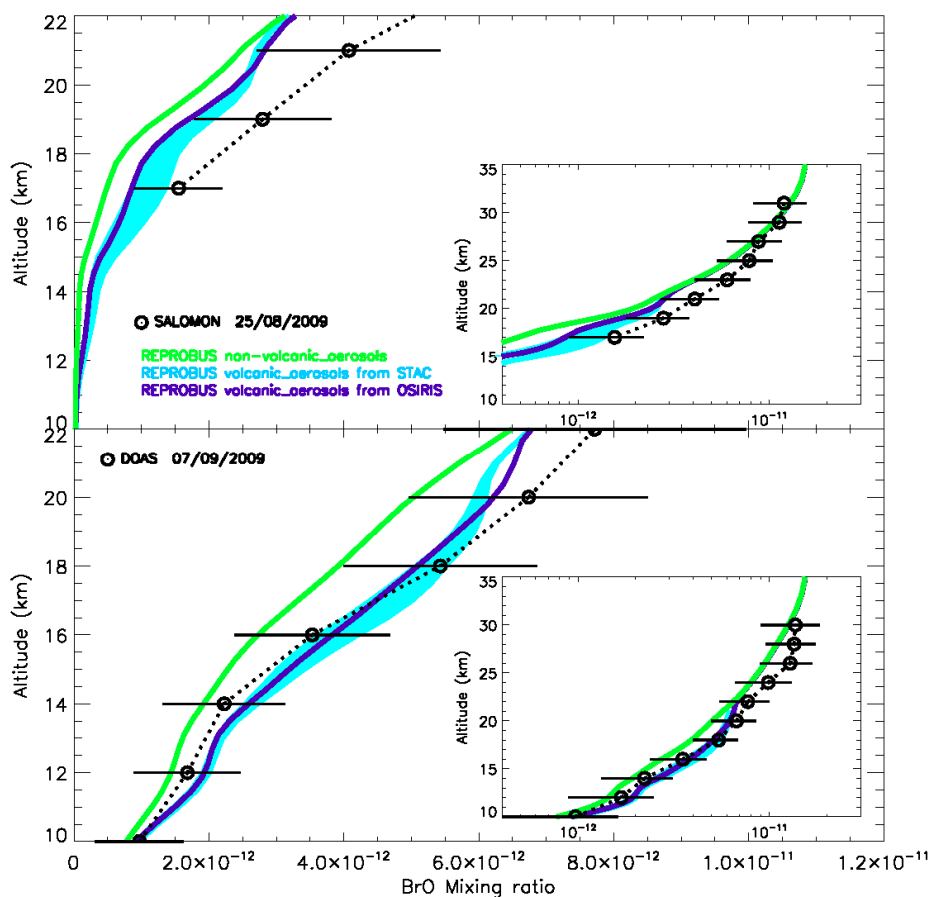


4  
5  
6  
7  
8  
9  
10  
11

**Figure 10:** same as **Figure 8** but for the  $\text{NO}_2/\text{HNO}_3$  ratio.



1  
2  
3

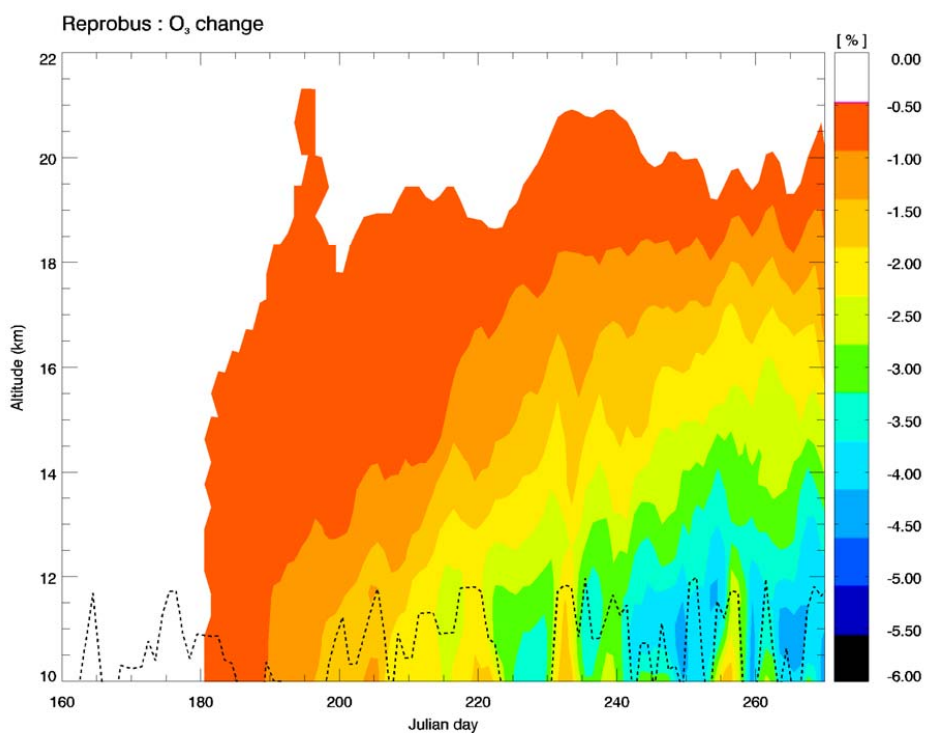


4  
5  
6  
7  
8  
9  
10  
11  
12

**Figure 11:** same as **Figure 7** but for BrO. The BrO profile from DOAS in the lower stratosphere has been obtained between 15:15 and 15:55 UT.



1  
2  
3



4  
5

6 **Figure 12:** Percentage changes in ozone over Kiruna (67.5°N, 21.0°E) as a function of altitude and  
7 time between 1 July and 1 October 2009. Calculations are done by subtracting outputs from the  
8 volcanic simulation driven by OSIRIS observations with the background simulation. The position of  
9 the tropopause is given by the black dotted line.